Distributed Optical Fiber Vibration Sensor Based on Phase-Sensitive Optical Time Domain Reflectometry

by

Meiqi Ren

Thesis submitted to the

Faculty of Graduate and Postdoctoral Studies

In partial fulfillment of the requirements for the

M.Sc. degree in Physics

Ottawa-Carleton Institute for Physics

University of Ottawa

Ottawa, Canada

To my family

Abstract

In this thesis, the work focuses on developing distributed optical fiber vibration sensors based on phase-sensitive optical time domain reflectometry (Φ-OTDR). Three works have been accomplished to improve the performances of Φ-OTDR for distributed vibration sensing.

Firstly, Φ-OTDR based on a polarization diversity scheme is demonstrated to mitigate the polarization mismatch effect occurring in traditional systems. A theoretical analysis is performed in different polarization cases corresponding to coherent and polarization diversity detection. Φ-OTDR based polarization diversity shows a great potential in the multi-events sensing application. Two vibration events are simultaneously detected and their signal to noise ratios are improved by 10.9 dB and 8.65 dB, respectively, compared to the results obtained by a conventional coherent scheme.

Intensity fluctuation in a phase-sensitive optical-time domain reflectometry (Φ-OTDR) system caused by stochastic characteristics of Rayleigh backscattering has limited relative vibration strength measurement, which is proportional to dynamic strain. A trace-to-trace correlation coefficient is thus proposed to quantify the Φ-OTDR system stability and a novel approach of measuring the dynamic strain induced by various driving voltages of lead zicronate titanate (PZT) is demonstrated. Piezoelectric vibration signals are evaluated through analyzing peak values of the fast Fourier transform spectra at fundamental frequency and high-order harmonics based on Bessel functions. Experimental results show high correlation coefficients and good stability of our Φ-OTDR system, as well as the small measurement uncertainty of measured peak values.

To reduce the intra-band noise caused by the finite extinction ratio of optical pulses, Φ-OTDR based on high extinction ratio generation is studied. Two methods are developed for achieving high extinction ratio of optical pulse generation. One of the approaches is to synchronize two cascaded electro-optic modulators to achieve high extinction ratio operation. The other one is to use the nonlinear optical fiber loop mirror as an optical switch to suppress the continuous wave portion of optical pulse. The sensing range of 1.8 km and 8.4 km with corresponding spatial resolution of 0.5 m and 2 m have been demonstrated based on cascaded two electro-optic modulators and nonlinear optical fiber loop mirror setup, respectively.

Acknowledgement

I would like to thank everyone who contributed to this thesis and helped me during my Master study. Firstly to my supervisor Prof. Xiaoyi Bao, for offering me the opportunity to have my Master study in her group. With her unconditionally support, I experienced a great time during the Master study. Her strong passion, diligence and persistence for research work set me a good example of not only doing the research but also the work in the future. Her insightful instructions and guidance helped me for fulfilling my research topics. I would also express my gratitude to Prof. Liang Chen for his instructive and suggestions during my research process. His critical thinking and profound knowledge in physics impress me and help me a lot for understanding the physics concepts.

Secondly, I would like to thank Dr. Ping Lu for his detailed guidance, useful instructions and precise modification. His expertise in the fiber optical technology helps me to improve the quality of the thesis work. This thesis would be impossible without his constant guidance.

Many thanks are given to Dr. Dapeng Zhou, who helps me for developing the experiment of nonlinear optical loop mirror for high extinction ratio of optical pulse generation.

I would like to thank Dr. Chams Baker who teaches me a lot in the experiment techniques and Mr. Jia Song who instructs me to build Φ-OTDR system at the beginning of my Master study. I also want to thank Dr. Yang Lu for his useful discussions and suggestions during my research process.

I shall give the special thanks to Mr. Yanping Xu, Mr. Dao Xiang and Mr. Song Gao who help me a lot during the courses we attended together.

I am thankful to all other colleagues in this lab: Prof. Zhonghua Ou, Dr. Yang Li, Mr. Bhavaye Saxena, Prof. Chunhua Wang, Ms. Qian He, Dr. Daisy Williams and Prof. Mingjiang Zhang. My life in the laboratory was enriched by their company.

Lastly, I shall sincerely thank my parents and my fiancé, for their support, love, encouragement and understanding through the years. This thesis is dedicated to them.

Statement of originality

This work contains no material which has been accepted for the award of any other degree or diploma in any university or other tertiary institution and, to the best of my knowledge and belief, contains no material previously published or written by another person, except where due reference has been made in the text.

I give consent to this copy of my thesis, when deposited in the University Library, being available for loan and photocopying.

SIGNED: ……..

DATE: ……...

Supervisor: Prof. Xiaoyi Bao

Contents

List of Figures

List of Acronyms

Φ-OTDR	phase sensitive optical time domain reflectometry
FFT	fast Fourier transform
ER	extinction ratio
EOM	electro-optical modulator
CW	continuous wave
FBG	fiber Bragg gratings
MZI	Mach-Zehnder interferometer
SI	Sagnac interferometer
FPI	Fabry-Perot interferometer
OTDR	optical time domain reflectometry
BOTDA	Brillouin optical time domain analysis
BOTDR	Brillouin optical time domain reflectometry
SNR	signal to noise ratio
PC	polarization controller
SMF	single mode fiber
P-OTDR	Polarization optical time domain reflectometry
SOP	state of polarization
PMD	polarization mode dispersion
DGD	differential group delay
OFDR	optical frequency domain reflectometry

FUT	fiber under test
LO	local oscillator
PMF	polarization maintaining fiber
MI	modulation instability
EDFA	erbium-doped fiber amplifier
PD	polarization diversity
PBS	polarization beam splitter
PDF	probability density function
ECL	external cavity laser
AOM	acoustic optical modulator
ASE	amplified spontaneous emission
DAQ	data acquisition card
PZT	lead zirconate titanate
NOLM	nonlinear optical fiber loop mirror
SHM	structural health monitoring

Chapter 1

1 Introduction

This chapter provides a review of the distributed optical fiber sensor technology. Special attention is paid to phase-sensitive optical time domain reflectometry (Φ-OTDR) for distributed vibration sensing. The motivation of this thesis is to optimize an Φ-OTDR system and improve sensing performances for practical applications. The contributions of the author to this thesis are presented in the section 1.2 and the thesis outline is described in section 1.3.

1.1 Background and motivation

1.1.1 Structural health monitoring

With the development of industrialized nations in recent centuries, it is difficult to imagine our lives without facilities such as railways, roads, bridges, tunnels, dams, etc. in our current world. These structures provide human beings with a better and more convenient life. However, these structures have their lifetimes and could deteriorate. The deterioration is commonly the result of aging of materials, overloading and lack of sufficient maintenance. Some examples of sudden collapse of structures can be found worldwide [1, 2]. Thus, to ensure structural safety and prevent disasters in advance, civil structures have to be equipped with structural health monitoring (SHM). SHM provides an effective tool to assess structural health conditions and help to avoid losses for users due to structural failure. Among the various sensing technologies, optical fibers with advantages such as lightweight and immune to electromagnetic interferences, are the most promising technologies for SHM. An effective SHM system should be real time and be able to detect various locations at the same time. The distributed optical sensors provide a more practical

and cost effective solution for large civil structures than discrete point sensors. The distributed sensors can determine the value of an object variable in a continuous way.

1.1.2 Distributed optical fiber sensors

In distributed optical fiber sensors, the whole fiber acts as multiple sensors that are sensitive to the environmental variables. The key idea of these sensors is to monitor the backscattered light spatially along the optical fiber. Typically, there are three types of backscattering occurring simultaneously in the optical fiber : Rayleigh, Brillouin and Raman [3]. Figure 1.1 shows the spontaneous scattering spectrum in the optical fiber. The Rayleigh scattering is an elastic scattering and the frequency of the scattered light is the same as the incident light. Brillouin and Raman scattering are inelastic scattering process and the frequency of the scattering light would shift a certain amount from the incident frequency. In the optical fiber, the frequency shift of the Brillouin scattering and Raman scattering is usually around 11 GHz and 13.2 THz, respectively.

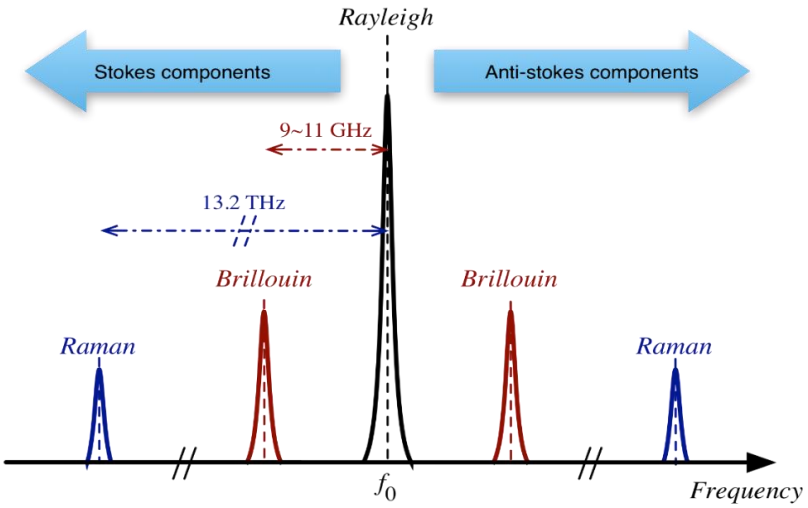

Figure 1.1 The spectrum of backscattered light in the optical fibers

The simplest distributed optical sensor is called optical time domain reflectometry (OTDR) which is based on Rayleigh scattering. OTDR is a common technology to measure the Rayleigh

backscattered light along the fiber length. It is widely used to estimate the attenuation of the fiber and measure the imperfections along the fiber. It also can be used for fiber length measurement, loss measurement induced by splice, micro bending, or connector etc. [4]. A distributed temperature sensing application based on OTDR has also been demonstrated in a liquid core fiber with an accuracy of 1˚C [5]. Polarization-OTDR (P-OTDR) has also been proposed by Rogers [6] by monitoring the state of polarization along the fiber. Although P-OTDR has been demonstrated for vibration sensing [7, 8], it is not easy for P-OTDR to detect multiple vibration points along the fiber because the state of polarization of the later optical signal would be disturbed by the previous vibration points. Another distributed optical fiber sensor based on Rayleigh scattering is optical frequency domain reflectometry (OFDR) which was attracted much interest in recent years because of its high spatial resolution and sensing accuracy. An OFDR system has been demonstrated for temperature and strain sensing with a 35 uε and 3.5 ˚C spatial resolution [9]. Vibration measurement has also been demonstrated based on time-resolved OFDR with the measurable frequency range of 0~32 Hz and spatial resolution of 10 cm [10].

In Brillouin based distributed sensors, external disturbances would change the Brillouin frequency shift, so temperature or strain measurements can be performed by monitoring the frequency shift of the Brillouin scattering. To overcome the weak spontaneous Brillouin scattering, a schematic based on stimulated Brillouin scattering has been proposed, named Brillouin optical time domain analysis [11-14]. It utilized two counter-propagating lasers with a Brillouin frequency shift and the Brillouin amplification process. Another schematic also related to Brillouin scattering is called Brillouin optical time domain reflectometry [15-17]. This approach is performed with a coherent detection to detect the weak Brillouin backscattering. The advantage of this setup is that it allows monitoring with one end of the fiber compared to the BOTDA system. Raman OTDR is

usually for temperature sensing because the intensity of the Raman scattering is a function of temperature [18, 19].

1.1.3 Φ-OTDR historical perspective

The Φ-OTDR designation is commonly used in the literature to refer to OTDR with use of highly coherent light. Φ-OTDR was initially demonstrated by Henry F. Taylor in 1993 for distributed optical intrusion sensing [20]. The system utilizes coherent spikes that are sensitive for external disturbances and previously regarded as fading noise in OTDR system. The coherent spikes come from the interference between Rayleigh backscattered light of different scattering centers within the pulse width. Then Φ-OTDR has been investigated and experimentally demonstrated by the same authors for intrusion sensing [21]. Although the performance of 1 km spatial resolution and 12 km sensing range were rather moderate, this field test is very important and presents a clear illustration of Φ-OTDR for practical applications.

After the initial demonstration of Φ-OTDR for intrusion sensing, it has been extensively studied for both intrusion and vibration sensing [22-24]. The vibration is usually induced by using a piezoelectric element or a mechanical actuator. In this case, the signal is analyzed in the frequency domain to obtain the vibration frequency. Many different schemes have been proposed in the literature to improve the performance of Φ-OTDR for dynamic measurements. The initial scheme of Φ-OTDR for intrusion sensing is based on direct detection with a low signal to noise ratio (SNR). The improvement of SNR and sensitivity has been made by using coherent detection for vibration sensing [22]. Besides these schemes, there are several signal processing methods used in an Φ-OTDR system to reduce the trace fluctuations caused by thermal noise, frequency drift of laser and instability of electronic equipment. The moving average and moving differential method is one common strategy [25] but the measured vibration bandwidth would be reduced in this

situation. To improve the vibration bandwidth, the wavelet denoising method has been introduced to Φ-OTDR. The experimental results show that a vibration event of a lead zirconate titanate (PZT) cylinder with a frequency as high as 8 kHz and 0.5 m spatial resolution can be detected in the single mode fiber [23]. The successful implementation of vibration sensing using Φ-OTDR provides a powerful tool to monitor the intrinsic frequency of civil structures which can identify and prevent internal damages at an early age.

Through many years' efforts made by researchers, Φ-OTDR has become an effective tool for distributed vibration and intrusion sensing. However, there are still some challenges in Φ-OTDR because trade-off of parameters could affect the performance of sensor systems and limit it to some applications. One of the biggest challenges is that polarization mismatch occurs in the coherent detection. This effect could reduce the probability of detecting vibration points and result in wrong pinpoints. Also, long range sensing is desired in some applications such as pipeline security monitoring. Sensing range of Φ-OTDR is limited by the input pulse energy, and the SNR in the rear end of the fiber is too low to detect the vibration. The sensing range can be extended by sacrificing the spatial resolution, but low spatial resolution could decrease sensing accuracy. Obtaining ae long sensing range and high spatial resolution at the same time is another challenge for Φ-OTDR system. Except for vibration frequency measurements, monitoring dynamic properties such as small amplitude movements is also essential to determine the extent internal damages to civil structures. It is difficult because of amplitude fluctuations of Φ-OTDR traces, which could result in huge measurement uncertainty. Considering these challenges in Φ-OTDR system, the aim of this thesis is to optimize the sensor system to improve its performance.

1.2 Thesis contributions

In this thesis, three main works have been performed for improvements of distributed vibration sensors based on Φ-OTDR in terms of different applications. The contributions are summarized in the following:

- The polarization diversity (PD) scheme based on Φ-OTDR system is developed to eliminate the polarization mismatch effect occurred in coherent detection. Φ-OTDR was firstly demonstrated with direct detection in which the Rayleigh backscattered light was directly monitored. Due to the weak Rayleigh backscattering, coherent heterodyne detection was then introduced to improve the SNR of the sensor system. However, the polarization mismatch between the sensing arm and the reference arm could deteriorate the detected signal at some positions along the fiber which makes these locations become insensitive to vibration. In the traditional setup, the polarization controller is introduced to match the polarization of two arms at the vibration position. But as the number of vibration events increases, it becomes difficult to align the polarization at all the positions at the same time by only adjusting the polarization controller. The use of polarization diversity method could mitigate the position dependent polarization fading effects and improve the overall SNR of the interference signal. This proposed sensor technique has great potential for multi-events detection and real distributed sensing.
- Up to now, Φ-OTDR sensors have been mostly demonstrated for distributed vibration sensing to identify the vibration location and frequency. Estimating dynamic strain from vibration measurement is also important for many applications. But due to the stochastic feature of the intensity fluctuations of Φ-OTDR traces, the amplitude measurement becomes a challenge

compared to the frequency measurement. Minimizing the intensity fluctuation and stabilizing the sensor system is a prerequisite for amplitude measurement. The use of a narrow linewidth laser with stable frequency and small phase noise could dramatically decrease the noise in an Φ-OTDR system. The system noise is quantified by calculating the trace-to-trace correlation and the average value of correlation coefficients of 0.9 is obtained in the experiment. Based on the above considerations, a technique for piezoelectric vibration amplitude measurement in Φ-OTDR system is demonstrated. By analyzing the peak value of the FFT spectrum at the fundamental frequency and high-order harmonics, the particular vibration modulation amplitudes have been extracted within a certain range determined by the Bessel functions.

- In an Φ-OTDR system, the extinction ratio (ER) of an optical pulse generated by the electro-optic modulator is finite and around 30~40dB. Intra-band noise is generated by the interference between the Rayleigh backscattered light induced by the continuous wave and the optical pulse. This would decrease the SNR of the detected signal and makes it difficult for long range and high spatial resolution sensing applications. Thus, high ER optical pulse is required in Φ-OTDR system with high performance. To resolve this problem, two different methods for achieving high ER of optical pulses have been developed. The ER of an optical pulse can be effectively improved by synchronizing two EOMs but at the expense of high insertion loss and increased complexity of the scheme. Another approach has also been demonstrated to achieve similar performance based on a nonlinear fiber loop mirror as an optical switch. Vibration sensing is achieved with 8.4 km sensing range and 2 m spatial resolution in this experiment.

1.3 Thesis outline

This thesis is divided into 6 chapters and organized as follows:

Chapter 1 presents the introduction of the work including the background, motivation and the main contributions of this thesis.

Chapter 2 focuses on the background introduction of the Φ-OTDR sensor system, where the principles, detection methods and the sensing performance are discussed.

Chapter 3 proposes the polarization diversity scheme based on Φ-OTDR for multi-events detection. The polarization fading effect in the fiber, motivation of this work, a theoretical statistical analysis, and experimental results are demonstrated in detail.

Chapter 4 presents a technique for measuring the piezoelectric vibration amplitude in Φ-OTDR. The system stability, the operation principles, the simulation analysis and experimental results are all discussed.

Chapter 5 proposes two methods for improving the extinction ratio of optical pulses generated by an EOM. Both dual EOMs and nonlinear loop mirror configurations are demonstrated in detail in Φ-OTDR to improve the sensing performance.

Chapter 6 concludes all the work in this thesis and gives some suggestions for future work.

Chapter 2

2 Phase-sensitive optical time domain reflectometry

Distributed vibration sensors provide a very effective way in structural health monitoring (SHM) to detect potential critical damages of civil structures and industrial machines. Among the different distributed fiber optical techniques, Φ-OTDR sensors show a good capability for monitoring vibrations. This chapter will present the background knowledge of phase-sensitive OTDR systems including the principle, detection methods, related noises, and sensor performances.

2.1 Rayleigh scattering in the optical fiber

Rayleigh scattering is caused by inhomogeneity of the fiber medium. The random ordering of the molecules causes localized variations of density and therefore fluctuations of the refractive index. Rayleigh scattering is an elastic scattering and the frequency of scattered light is same as the incident light. Rayleigh scattering [26] is the most important factor for determining the transmission loss of an optical fiber. Rayleigh scattering in a silica glass is caused by the density fluctuations frozen into the fused silica during the manufacturing process. It results in the refractive index change along the fiber. The intrinsic loss coefficient of the optical fiber due to Rayleigh scattering is expressed as

$$\alpha_s = C / \lambda^4 \tag{2.1}$$

where C is in the range of 0.7-0.9 dB/(km-μm^4) depending on the constituents of the fiber core [27]. Rayleigh scattering and material absorption are two mechanisms for the fiber loss. The total attenuation coefficient is denoted as α (with the units of km^{-1}). In the wavelength 1550 nm which

is commonly used in the optical communication, the attenuation coefficient is 0.2 dB/km in the standard single mode fiber (SMF). Considering the scattering coefficient in the range 0.12-0.16 dB/km, Rayleigh scattering is the dominant loss near that wavelength. This provides a way to estimate the fiber attenuation by monitoring the Rayleigh backscattering power.

Due to the attenuation loss, the input optical power will decay exponentially as a function of the propagating distance z as shown in the following equation:

$$P(z) = P_0 \, \mathrm{e}^{-\alpha z} \tag{2.2}$$

where P_0 is the power of the incident light. P(z) is the transmitted power at distance z. In equation 2.2, the unit of α is km^{-1}. The attenuation coefficient α can also be expressed in the unit of dB/km for convenience in practice. Then the transmitted power can be written as:

$$P(z) = P_0 10^{-\alpha_{\mathrm{dB}} z/10} \tag{2.3}$$

with $\alpha_{\mathrm{dB}} \approx 4.34\alpha$.

2.2 Optical time domain reflectometry (OTDR)

2.2.1 Pulse generation in OTDR

In an OTDR system, an optical pulse is used to obtain distributed spatial information along the fiber. The optical pulse is usually generated by using an external electro-optical modulator (EOM). The most popular material used in the EOM is $LiNbO_3$ which has a relatively high linear electro-optic coefficient α_{EO}. The refractive indices of the material are a function of the applied electrical field and the index change is linearly proportional to the applied field magnitude. The optical phase change introduced by the linear electro-optic effect is [28]:

$$\phi(V) = \frac{2\pi\alpha_{\mathrm{EO}} L}{\lambda d} V \tag{2.4}$$

where L is the length of the electrode, the separation between the two electrodes is d and the applied voltage is V. An intensity modulator can be made based on the same electro-optic effect by utilizing the balanced Mach-Zehnder interferometer configuration. The electrical field is applied across one of the two arms to introduce an additional phase delay and control the phase difference of the two arms. Then the output optical signal is an interference signal and the transfer function is [28]:

$$T(V) = \cos^2\left(\phi_0 + \frac{\pi V}{2V_\pi}\right) \tag{2.5}$$

where

$$V_\pi = \frac{\lambda d}{2\alpha_{\mathrm{EO}} L} \tag{2.6}$$

ϕ_0 is the initial phase difference between two arms without applying the voltage. The value may change with temperature and manufacturing tolerances. A bias voltage is usually introduced to adjust ϕ_0 for different applications. In the application of pulse generation, the bias voltage works at the minimum point of the transfer function and the time dependent electrical pulse is added into the RF input of an EOM. The working principle of pulse generation is illustrated in figure 2.1.

The extinction ratio (ER) is an important parameter of an EOM for pulse generation, which is defined as the ratio of output power at on state to the output power at off state. Thus, the peak electrical voltage is adjusted to have the same value of V_π in order to get the maximum ER. However the transmission power cannot reach to the minimum point of the EOM transfer function because of the refractive index distortions in the electro-optic crystals that impart wave front distortion to the optical beam. This could limit the ER of the EOM and the commercial ER of an EOM is usually around 30~40dB.

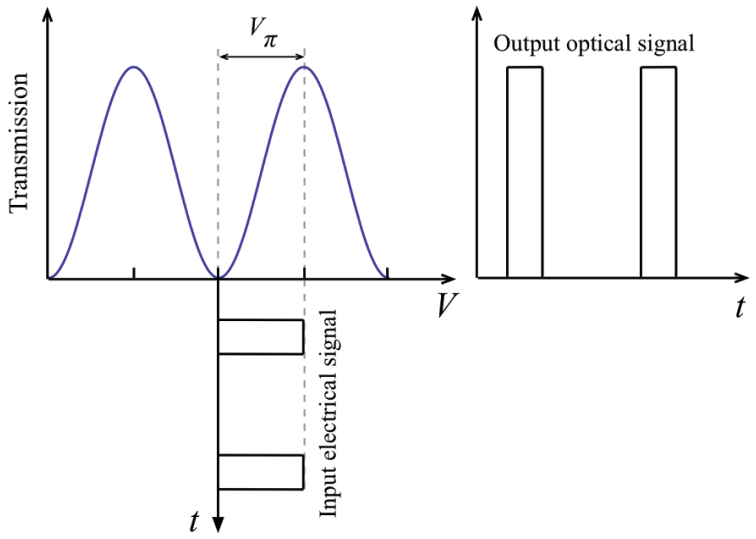

Figure 2.1 Operation principle of pulse generation by EOM

2.2.2 OTDR principle of operation

A simplified OTDR setup is shown in figure 2.2. The laser source used in an OTDR system is a broadband light source which is modulated by an EOM to generate optical pulses. Then the optical pulses are sent into the sensing fiber through a circulator, and the Rayleigh backscattered light is detected by a photodetector (PD). The detected optical power decreases exponentially (linearly in dB unit) with respect to the distance along the fiber and shows abrupt peaks and dips at the location of connectors, bend and breaks due to Fresnel reflections at the end of fiber which are shown in figure 2.3.

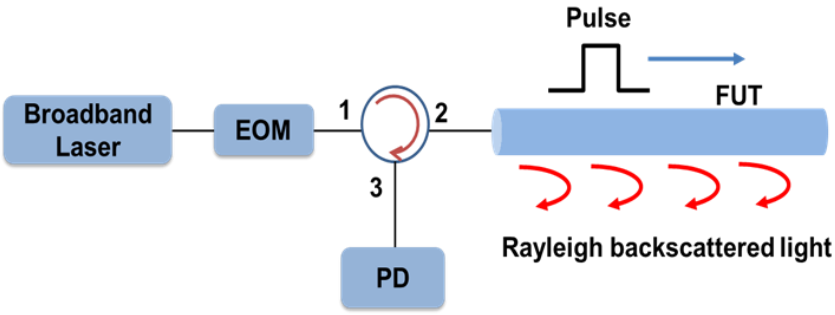

Figure 2.2The simplified configuration of OTDR system

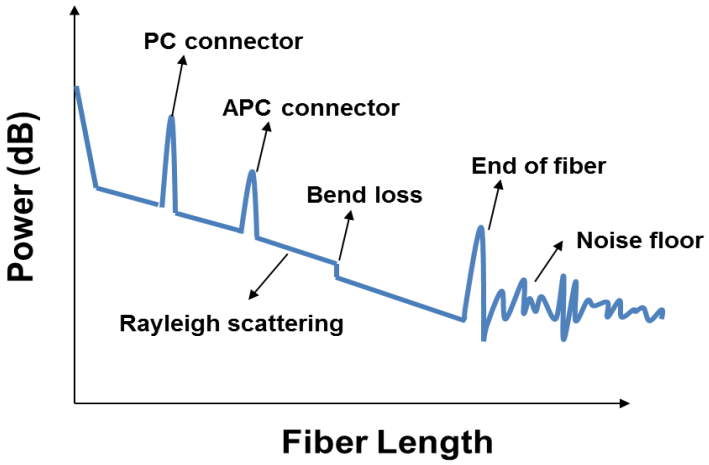

Figure 2.3 The illustration of OTDR trace

In order to avoid the superposition of backscattered signals, only one pulse is sent into the fiber at a time. Thus, the repetition rate of optical pulse is limited by the fiber length and the time delay between the pulses is:

$$\tau = \frac{2L}{v_g} \tag{2.7}$$

where L is the distance from the input end, v_g is the group velocity of the light propagating in the optical fiber. In the OTDR system, the spatial resolution and dynamic range are two most important parameters characterizing the performances of system. The spatial resolution Δz, which is the minimum resolvable distance, determined by the width of the launched pulse such that:

$$\Delta z = \frac{T_p v_g}{2} \tag{2.8}$$

where T_p is the pulse width of incident light. When the attenuation is constant for both directions of propagation, the backscattered power, P_{bs} can be calculated as [29]:

$$P_{bs} = \frac{F a_s T_p v_g P_0 e^{-2\alpha L}}{2} \tag{2.9}$$

where a_s is the Rayleigh scattering coefficient, a is the fiber attenuation coefficient, F is the capture coefficient and P_0 is the input power.

The dynamic range is defined as the difference between the initial backscattered power level and the noise level of a measurement time. The way to increase the system's dynamic range is either to enhance the backscattered power or to decrease the noise level. From equation (2.9), the backscattered power is proportional to the product of pulse width T_p and input power P_0. However in the OTDR system, the pulse with very high peak power is not desired because it will cause the nonlinear effects in the fiber. So the dynamic range mainly depends on the pulse width. Increasing the dynamic range requires the longer pulses which would decrease the spatial resolution as defined in equation (2.8). This trade-off between the dynamic range and spatial resolution represents the fundamental limit of the OTDR system. Thus, designing the system needs to consider both parameters tailored to different applications.

2.3 Φ-OTDR

2.3.1 Principle of Φ-OTDR

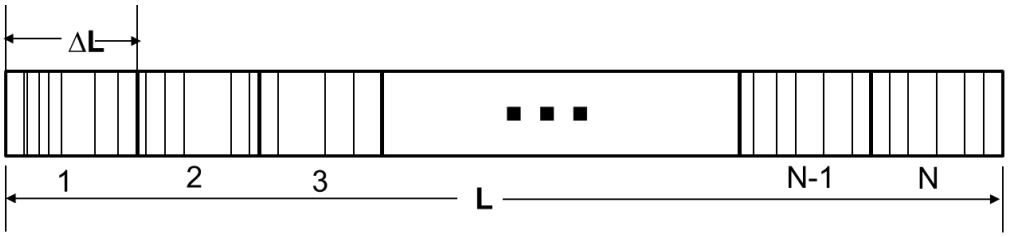

Figure 2.4 The schematic of simulation model of Φ-OTDR system

Φ-OTDR configuration is very similar with OTDR besides that the laser source is a narrow linewidth laser whose coherent length is much longer than the fiber length. In order to understand the principle of Φ-OTDR, a simplified simulation model has been developed [30] and the

schematic is shown in figure 2.4. The Rayleigh backscattered light can be modeled as a sequence of scattering centers. These scattering centers can be seen as multiple reflectors with weak reflectivity. The fiber can be divided into N small sections and the length for each section is $\Delta L=L/N$. ΔL can be seen with the same length as the pulse width in the simulation. In each section of the fiber, there are M scattering centers which are randomly located with the uniform distribution. So the electric field of Rayleigh backscattered light can be written as:

$$E_{\mathrm{bs}}{}^{i} = E_0 \exp(-2\alpha L_i)\sum_{k=1}^{M} r_k^i \exp(j\varphi_k) \tag{2.10}$$

where α is the attenuation coefficient of the optical fiber, L_i is the length of the i^{th} section of the fiber and $L_\mathrm{i}=i\Delta L$. r_k and φ_k are the scattering coefficient and phase of k^{th} scattering center, respectively. In Φ-OTDR, backscattered light within the pulse width will interfere each other and form a random interference pattern. Here we can assume the scattering coefficient for every scattering center is the same, denoted by r. Then intensity of the detected signal can be expressed as:

$$I_{\mathrm{bs}}{}^{i} = \left|E_{\mathrm{bs}}{}^{i}\right|^2 = \sum_{k=1}^{M-1}\sum_{k'=k+1}^{M} E_0{}^2 r \exp(-4\alpha L_i) + 2E_0^2 r^2 \sum_{k=1}^{M-1}\sum_{k'=k+1}^{M} \cos(\varphi_{k'} - \varphi_k). \tag{2.11}$$

The first part of the detected signal is the DC component which is not our main interest. The second term is the sum of multiple interference signals and its intensity depends on combination of the phase difference within the pulse width.

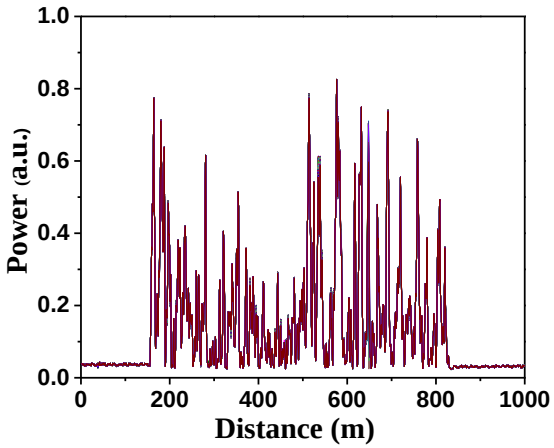

Figure 2.5 Typical trace obtained by Φ-OTDR system

From equation (2.11), the intensity of detected signal is related to the relative phases of reflected light coming from different scattering centers within the pulse width. Since the scattering centers are randomly distributed along the fiber, the Φ-OTDR traces typically have random oscillating features, which is shown in figure 2.5. This random pattern remains same over time if the scattering centers do not suffer from any changes. If there is any disturbance at one certain location, the relative phases of backscattered light are changed and Φ-OTDR traces will vary at that disturbance location. Thus, the disturbance location can be obtained by tracking the difference between un-perturbed and perturbed signals or by traces subtraction. In the case of vibrations, the Φ-OTDR traces will show local variations synchronized with the vibration frequency. 100 superposition of Φ-OTDR traces around vibration location is shown in figure 2.6(a). The intensities at other locations are almost the same for every trace but only around 650 m varies from trace to trace due to the vibration. After subtracting adjacent traces, the vibration location is clearly shown in figure 2.6(b). The vibration frequency can be obtained by performing the fast Fourier transform at vibration location along the sequence traces.

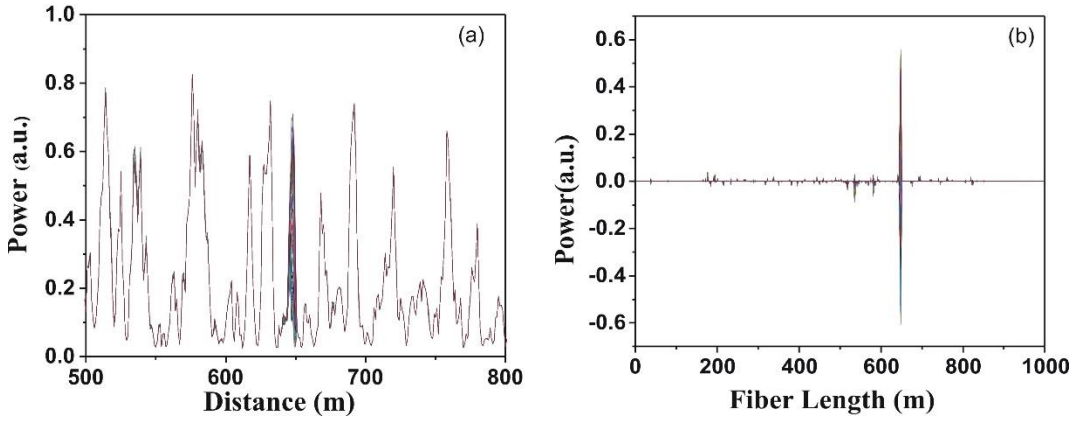

Figure 2.6 (a) Φ-OTDR traces with the vibration at 650 m; (b) the vibration location after traces subtraction

2.3.2 Detection methods and noise in Φ-OTDR

2.3.2.1 Direct detection

The operation principle and schematic of Φ-OTDR with a direct detection are as described in section 2.3.1. The direct detection scheme presents the low complexity in which the signal is directly detected in the time domain. It is usually suitable for the short range sensing measurements where the backscattering light is relatively strong. There are several noise sources in the direct detection including laser phase noise, laser frequency drift, and intra-band noise caused by the finite extinction ratio of the optical pulse. The laser phase noise is determined by the linewidth of the laser which could affect the performance of Φ-OTDR for vibration sensing [31]. In order to reduce the fluctuation of phases, the coherence length of laser should be longer than the pulse width. The laser frequency drift would also cause the fluctuation of Φ-OTDR traces since the interference patterns would change in different laser frequencies [32]. Therefore, in order to get stable traces in Φ-OTDR, the system not only requires the high coherent laser but also the laser with stable frequency over the measurement time. The active compensation method that utilizes the laser frequency sweeping and cross-correlation calculation has been proposed to suppress the trace distortion [33]. Beside these two factors, the fluctuation of traces can also be introduced by

EOM. In the experiment, the EOM bias is easily drifted during the long time operation and it would decrease the ER of optical pulse. This will result in a CW component between pulses and generate a CW backscattered light that would decrease the SNR. Because the CW noises are accumulated with the fiber length, it could limit Φ-OTDR to long range and high spatial resolution sensing applications. The EOM feedback control in Φ-OTDR is introduced for solving the bias drift problem [34]. The approaches of improving ER of optical pulse will be discussed in Chapter 5 in this thesis.

2.3.2.2 Coherent detection

Due to the weak Rayleigh backscattering in optical fiber, the use of coherent detection can greatly increase the SNR and sensitivity of a detected signal. The principle of coherent detection consists of mixing the optical signal with a local oscillator (LO) before it reaches the photodetector. A schematic of Φ-OTDR with coherent detection is shown in figure 2.7.

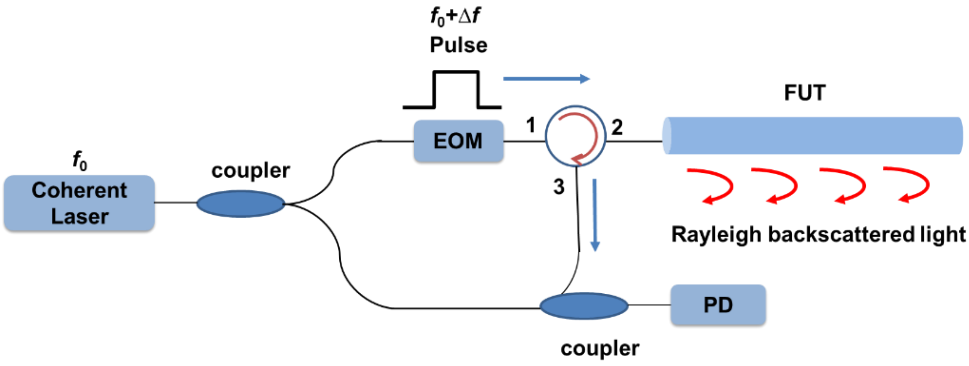

Figure 2.7 The schematic of Φ-OTDR based on coherent detection

The light coming from a laser with a frequency f_0 is split by an optical coupler into two arms. One arm is used as LO and the other is used for generating the backscattered signal. In coherent detection, the frequency of optical pulses are usually shifted Δf (usually few hundreds MHz) before sending into the fiber. In this case, the detected signal becomes the interference

between the LO and the Rayleigh backscattered light. Because the optical amplitude of LO signal is typically much higher than that of the backscattered signal, the intensity of interference signal in this case will be higher than that in the direct detection. If the optical amplitude of LO is high enough, the SNR of coherent detection can be reached to shot noise limit even for weak signals, while the direct detection cannot achieve this. Therefore, the coherent detection is more suitable for weak signal detection compared to direct detection.

The main disadvantages of using coherent detection are higher noises and instability of Φ-OTDR traces. Beside the noise occurring in the direct detection, the coherent detection is much more sensitive to the phase noise and strongly dependent on the state of polarizations of two arms. In the coherent detection, the polarization mismatch between two arms can deteriorate the interference signal at some positions. By using the polarization maintaining fiber (PMF), as well as polarization maintaining components, the polarization dependent problem has been solved [24]. But PMFs are expensive and have relatively high loss which limits the sensing range when compared to the use of SMF. The polarization diversity detection could also solve this problem and the details will be presented in the chapter 3.

2.3.3 Vibration sensing performance

The good visibility and high SNR in the measured traces in Φ-OTDR are required to achieve reliable vibration measurements. The high spatial resolution, long sensing range, and wide frequency bandwidth are always desired in the distributed vibration sensing. These parameters are tightly related, however. In vibration sensing, the sensing range is restricted by the repetition rate of optical pulses because it requires only one pulse traveling in the fiber at a time. Thus low repetition rate is needed for the long range measurement. However, the maximum resolvable vibration frequency is also determined by the repetition rate in the Φ-OTDR. The maximum

frequency response is half of the repetition frequency of optical pulse according to the Nyquist sampling theorem. The tradeoff between the long sensing measurement range and high frequency response limits Φ-OTDR to high frequency vibration measurement. Several techniques have been proposed to break this limit. The repetition rate is enhanced by using the dual frequency pulses [35]. In this case, the dual pulses with different frequencies with a time delay are sent into the fiber simultaneously. The superposed traces can be demodulated by different beat frequencies. The maximum frequency is improved by a factor of 2 by using this method. The high frequency measurement can also be achieved by combing the MZI and Φ-OTDR [36] . In this configuration, the Φ-OTDR is used to locate the vibration position and the MZI will give the vibration frequency information which is not restricted by the repetition rate of optical pulse. The technique allows the detection of distributed frequency vibrations of up to 6 MHz of a pencil break event over 1 km of fiber with 5 m spatial resolution. But only one vibration event can be measured in this case. In addition, the non-uniform sampling has also been demonstrated for vibration frequency response improvement [37].

The peak power in the Φ-OTDR also should be controlled properly because the high peak power of optical pulse would result in the nonlinearities which could degrade the performance of the system. The influence of modulation instability (MI) in Φ-OTDR operation has been studied [38]. MI in fibers results from the interplay of Kerr-effect and anomalous dispersion, and in time domain, results in the breakup of a CW beam into a train of ultra-short pulses. In the spectral domain, MI has two sidebands at each side of the center beam wavelength. But in the case that the wavelength is operated in the normal dispersion regime, MI effect is not the main limitation of peak power in Φ-OTDR system. Other nonlinearities such as Brillouin or Raman effects could also affect the system performances. Thus, it is difficult to achieve long sensing range measurement by

only increasing the pulse peak power.

To effectively increase the sensing range in Φ-OTDR, optical amplifications must be used. Although use of erbium-doped fiber amplifier (EDFA) for amplifying Rayleigh backscattered light would increase the sensing range, the signal still degrades after 10 km because of attenuation loss. However use of distributed amplifications would amplify the weak signal from end of the fiber which compensates the attenuation loss at rear end. Thus the distributed amplifying schemes provide a way in Φ-OTDR for long range measurements. The use of Brillouin amplification has been proposed to extend the sensing length of Φ-OTDR. The optical pulse and CW light with a frequency difference of Brillouin frequency is sent into the fiber at opposite ends of the fiber respectively. Then the CW light will transfer the energy to the optical pulse at the remote end of the fiber because of the SBS process. The sensing range over 100 km has been demonstrated by using this method [39]. Beside Brillouin amplification, the first order and second order Raman amplification for long range sensing measurement have also been demonstrated [40, 41].

Chapter 3

3 Polarization diversity scheme in phase-sensitive OTDR for multi-events vibration detection

Φ-OTDR systems have been widely used for distributed vibration sensing. However, polarization fading affects the reliability of the sensors. This chapter presents an Φ-OTDR based on a polarization diversity (PD) scheme to compensate the position dependent polarization fading occurring in the coherent detection. A real distributed vibration sensing for multi-events detections can thus be achieved along each position along the sensing fiber with more reliable vibration measurements results. The experiment shows that the SNR of two vibration signals are simultaneously enhanced by 10.9 dB and 8.65 dB compared to the results obtained by a conventional coherent detection scheme. Section 3.1 gives the introduction of this work. The polarization fading effect is discussed in section 3.2. Section 3.3 presents the theoretical analysis of interference signals in the Φ-OTDR system under the various polarization states. Section 3.4 demonstrates the experiment details of the PD scheme in the Φ-OTDR including the set-up (3.4.1) and the experimental results and discussions (3.4.2). The last section 3.5 is the conclusion.

3.1 Introduction

Fully distributed optical fiber sensors (DOFS) have been extensively studied because of their advantages over the traditional point sensors. The DOFS developed based on Brillouin scattering in optical fiber have been successfully demonstrated for static measurement, such as strain and temperature measurement [46, 47]. As for dynamic measurement, the distributed vibration sensors have broad applications in health monitoring and damage detection of civil infrastructures [8, 48].

The most promising technique to fulfill distributed vibration measurement is Φ-OTDR due to its advantages such as high sensitivity, large dynamic range and simple configuration.

The Φ-OTDR system operates based on coherent Rayleigh scattering light by utilizing a high-coherence laser with narrow line-width. The detected signals are induced by the interference between multiple Rayleigh scattering centers within a pulse width. External perturbations including acoustic waves or vibration applied on the fiber would modulate the effective refractive index of the guided optical mode, causing a phase shift of reflected light as well as the change in the intensity of detected signals. The Φ-OTDR was firstly realized using a direct detection scheme as an intrusion sensor with a simple setup, however a relatively low SNR was obtained [21, 49]. By using the post-signal processing methods such as moving average and wavelet denoising, the Φ-OTDR with high sensitivity and SNR has been demonstrated, which allows the acoustic wave and vibration spectrum to be measured in a distributed fashion [23]. The performance improvement in an Φ-OTDR system was achieved by using a heterodyne coherent detection technique [22]. However, the coherent detection is susceptible to the polarization mismatch between the measured and reference signals, and hence the measurement accuracy can be greatly affected by the polarization induced fading phenomenon [50] . The polarization mismatch would decrease the SNR of Φ-OTDR time-domain traces and cause the low visibility of interference signals. Unreliable vibration measurement results may occur at polarization mismatched locations because of these disturbance-insensitive regions.

For single-point sensing applications, a polarization controller is introduced in the reference arm to align the polarization at certain locations. For distributed sensing applications, since the state of polarization of Rayleigh backscattered light changes randomly along the low-birefringence optical fiber, it is impossible for the PC to keep polarization alignment for the backscattered signals

at each location along the sensing fiber. Thus the probability of finding the useful polarization matched locations could be significantly reduced. This problem becomes even more serious in multiple vibration events detection. It could be a major obstacle in real field such as intrusion detection, leakage detection of pipeline monitoring, internal crack of bridge and oil-well condition monitoring. To mitigate the polarization fading effect, one approach is to utilize the high-birefringence polarization-maintaining fiber configurations [24]. In spite of its high SNR and sensitivity, this configuration is not suitable for long range sensing (typically limited to 1 km) because of the high loss of the PMF as well as the corresponding higher cost of polarization-maintaining optical fiber components required in the systems. The PD method [51] provides an alternative solution for Φ-OTDR to reduce the polarization fading by separating the backscattering signals into two orthogonal polarization states through a polarization beam splitter (PBS), and then combine the two separated signals so that the detected signals are insensitive to the SOP in fibers. The polarization discrimination in an Φ-OTDR intrusion-sensor was achieved by utilizing the direct detection and PD scheme in the field tests [52]. Although the research on the PD scheme has been a focus in Brillouin scattering based DOFS [53, 54], it has not been thoroughly synthesized in Φ-OTDR.

3.2 Polarization effects in single mode fiber

The fundamental mode (HE_{11}) in the single mode fiber is a combination of two orthogonal polarization modes. In ideal fibers with perfect cylindrical symmetry and stress-free, the two modes are degenerate with the same propagation constants and any polarization state coupled into the fiber would not change during propagation. In practical fibers, mechanical and thermal stresses induced during the manufacturing process could break the circular symmetry of the ideal fiber and

result in a mixing of polarization states. The propagation constant becomes slightly different for the two orthogonal polarization modes because of the property of modal birefringence. The modal birefringence B_m in the optical fiber is defined as the difference between the effective refractive indexes of two orthogonally polarized states [27]:

$$B_m = \left| n_x - n_y \right| \tag{3.1}$$

where n_x and n_y are the modal refractive indices for the two orthogonally polarized states. Thus the effects of birefringence would cause a general polarization state to evolve through a periodic sequence of states as it propagates. This period is called beat length and defined as:

$$L_B = \frac{\lambda}{B_m} \tag{3.2}$$

Generally, the single mode fibers are expected to have birefringence of the order of 10^{-7}. The birefringence is usually not constant along the fiber but changes randomly because of the fluctuations in the fiber core. This could result in a random change of SOP during the propagation although a light with fixed linear SOP is launched into the fiber. This is not the issue in some applications as the detected signal is not sensitive to its polarization state. However, it is critical in fiber-optical interferometric sensors and coherent detection schemes. The polarization fading effects in the single mode fiber could reduce the visibility of detected signal, which should be considered carefully as developing the sensor system.

3.3 Theoretical analysis of different polarizations states in phase-sensitive OTDR

Figure 3.1 illustrates a simulation model for Rayleigh backscattering in a single-mode fiber that consists of a sequential series of spatially discrete low-birefringence reflectors with various

specifications. The variation of directions for principal birefringence axes of each reflector is presented over the length of the SMF because of inhomogeneous material density and fluctuation in the fiber ellipticity induced via fiber manufacturing process.

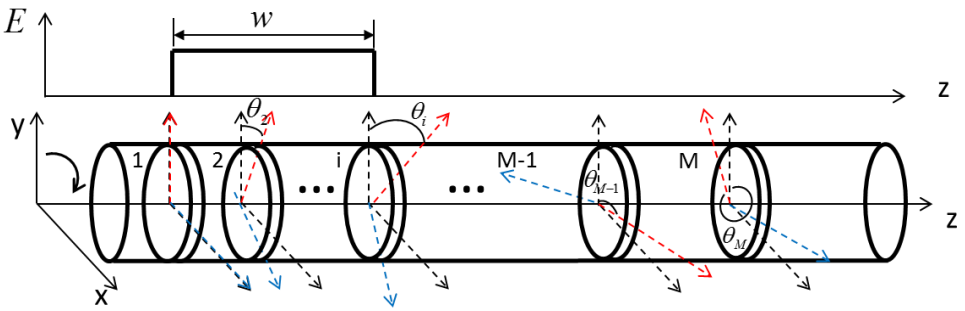

Figure 3.1. Illustration of randomly distributed reflectors along a SMF.

As illustrated in figure 3.1, a coordinate system is defined that x-axis and y-axis represent two equivalent principal birefringence axes (i.e., the slow axis and fast axis) of the SMF, respectively. When a pulse with a central frequency f_0 is injected into the sensing fiber, the electric field of the backscattered light at the fiber input end (z = 0) at time t is the sum of the electric field of every Rayleigh scattering centers over half of the pulse duration that is from (tv_g-w)/2 to tv_g/2, which can be expressed as

$$E_{t,z=0} = E_0 \sum_{z_j = tv_g/2 - w}^{tv_g/2} r_j e^{i\left(2\pi f_0 t + 2\beta z_j + \phi_j(t)\right)} e^{-2\alpha z_j}, \tag{3.3}$$

where E_0 is the initial electric field amplitude, v_g are respectively the group velocity, w is the spatial length of the pulse width, α and β are respectively the average attenuation coefficient and propagation constant. The subscript j represents the j-th reflector. r_j is the reflectance, z_j is the randomly distributed position, $\phi_j(t)$ is the time-dependent phase perturbation caused by internal instability of the Φ-OTDR and external disturbance on the sensing fiber. In the coherent heterodyne detection based Φ-OTDR, the input pulse will be modulated by an acoustic-optic modulator (AOM)

to introduce a frequency shift, and then reflected Rayleigh backscattering light is mixed with the reference light. The detected intensity will become:

$$I = \sum_{j=1}^{N} (E_0 r_j)^2 e^{-4\alpha z_j} + E_r{}^2 + 2\sum_{j=1}^{N} E_0 r_j E_r e^{-4\alpha z_j} \cos(2\pi \Delta f t + \Delta\phi_j(t)) \cos(\theta_j(t)), \quad (3.4)$$

where E_r is the electric field amplitude of reference arm.

The probability density function (PDF) of the Φ-OTDR output intensity is analyzed under the cases of polarization mismatch and polarization match. The analysis is based on speckle patterns as a random walk process [55]. Both the real and imaginary parts of the resultant electric fields for all Rayleigh scattering centers can be characterized as Gaussian random variables,

$$\begin{aligned} E_{\mathrm{Re}} &= \mathrm{Re}\{\sum_{j=1}^{N} A_j e^{i\Phi_j}\}, \\ E_{\mathrm{Im}} &= \mathrm{Im}\{\sum_{j=1}^{N} A_j e^{i\Phi_j}\}, \end{aligned} \quad (3.5)$$

where A_j and Φ_j are the amplitude and phase of the j-th reflector, respectively. In the polarization mismatch case, θ_j varies along the fiber, following the uniform distribution in the [0, 2π] interval. The reflected signals from uncorrelated Rayleigh scattering centers become independent from each other, leading to the statistical independence of the real and imaginary parts of the resultant electric field in equation (3.5). According to the central limit theorem, when N increases towards an infinite value, the joint probability density function of the real and imaginary parts of the random phasor sum can be expressed as

$$P_E = \frac{1}{2\pi\sigma^2} \exp\left(\frac{E_{\mathrm{Re}}^2 + E_{\mathrm{Im}}^2}{-2\sigma^2}\right), \quad (3.6)$$

where $\sigma = (NA^2/2)^{1/2}$, and A is the mean value of the electric field amplitude of each reflector. Then the PDF of the output intensity can be represented by a negative exponential function [56],

$$P(I) = \frac{1}{< I >} \exp(-\frac{I}{< I >}), \tag{3.7}$$

where <*I*> is the mean intensity. In the case of complete polarization match, the output intensity is an interference signal of different scattering centers with the same form of equation (3.4) except $\theta_j = 0$. The PDF of the output intensity can be shown as a normal distribution for the limit $N \rightarrow \infty$ [57]. In a partial polarization mismatch case, reflected light from different scattering centers does not completely interfere with each other due to reduced efficiency of the coherent detection, leading to a drop in the effective number of the scattering centers. Thus, the PDF of the output intensity in a practical Φ-OTDR comes between the above two limiting cases, and can be estimated by using a Gamma distribution [58, 59]:

$$P(I) = \frac{I^{k-1}}{\theta^k \Gamma(k)} \exp(-\frac{I}{\theta}), \tag{3.8}$$

where Γ is the gamma function with the shape and scale parameters of k and θ, respectively.

3.4 Experimental details of polarization diversity in phase-sensitive OTDR

3.4.1 Experiment setup

The experimental setup of the Φ-OTDR based on the polarization diversity scheme is shown in figure 3.2. The light source is an external cavity laser (ECL) with the central wavelength of 1550 nm and line-width of 50 kHz. The light was split into two paths by an 80:20 optical coupler. Then the 80% light beam in the sensing arm was sent into the acoustic optical modulator (AOM) with a frequency shift of 200 MHz and also modulated by an EOM controlled by a function generator. The modulated pulse was amplified by an erbium doped fiber amplifier (EDFA). After filtering the amplified spontaneous emission noise (ASE) from EDFA, the optical pulse was fed into the

sensing fiber through a circulator, and the Rayleigh backscattered light will combine with the reference light by a standard 50:50 optical coupler. In the PD scheme, the reference light was launched into a polarization beam splitter (PBS) at 45° via adjusting the polarization controller. And PBS separated the reflected signals from the sensing arm into parallel and perpendicular polarization states. Then the two orthogonally polarization signals from the PBS were independently detected by two balanced detectors and the recorded intensity can be respectively expressed as:

$$I_{//} = 2\sum_{j=1}^{N} E_0 r_j E_r e^{-4\alpha z_j} \cos\left(2\pi\Delta f t + \Delta\phi_j(t)\right)\cos\zeta,$$
$$I_{\perp} = 2\sum_{j=1}^{N} E_0 r_j E_r e^{-4\alpha z_j} \cos\left(2\pi\Delta f t + \Delta\phi_j(t)\right)\sin\zeta, \tag{3.9}$$

where ζ is the angle between the polarization state of Rayleigh backscattering light and the principal axes of the PBS. To mitigate the polarization fading noise, the perpendicular and parallel signals were firstly squared and then summed together. Then the signals became polarization independent and were recorded by a data acquisition card (DAQ).

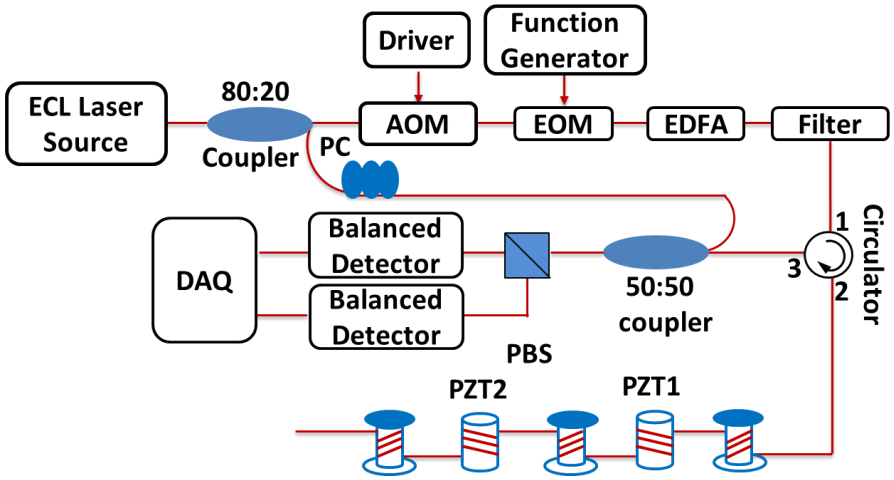

Figure 3.2 Φ-OTDR setup with the polarization diversity scheme

In the experiment, two lead zirconate titanates (PZTs) are used as vibration sources. A

section of fiber is attached to each PZT and distance between two PZTs is around 120 m. The working principle of PZT is that the circumferential change of piezoelectric material directly couples to the length change of the fiber under an applied electric voltage. Thus the phase delay is introduced through that section of fiber by changing its physical length and refractive index [60]. The response of these modulators is flat for frequencies between zero and the lowest resonate frequency. Resonate frequency is determined by the diameter of tube and material of the device, which is usually at tens kHz. Beside the phase change, a small amount of birefringence modulation is also introduced since the piezoelectric tube contacts only one side of the optical fiber and causes a modulated stress across the fiber. But the dominant modulation is phase modulation, the polarization modulation is approximately 0.1% of phase modulation [61] .

3.4.2 **Experimental results and discussions**

From our theoretical analysis, the output intensity of the Φ-OTDR would exhibit different distributions under the conditions of polarization mismatch and polarization match. Both simulated and experimental results of the intensity distribution along the fiber are shown in figure 3.3. The fitting curves in figure 3.3(a) and 3.3(b) are obtained by using exponential distribution. In figure 3.3(c) and 3.3(d), the Gamma distribution is used to fit the intensity distribution in the case of polarization match. The experiments were carried out with pulse width of 50 ns and input power of 10 mW based on the conventional coherent detection scheme and polarization diversity scheme, respectively. The average power of detected signal is increased and the intensity distribution tends to convert from exponential to gamma distribution by applying the PD method.

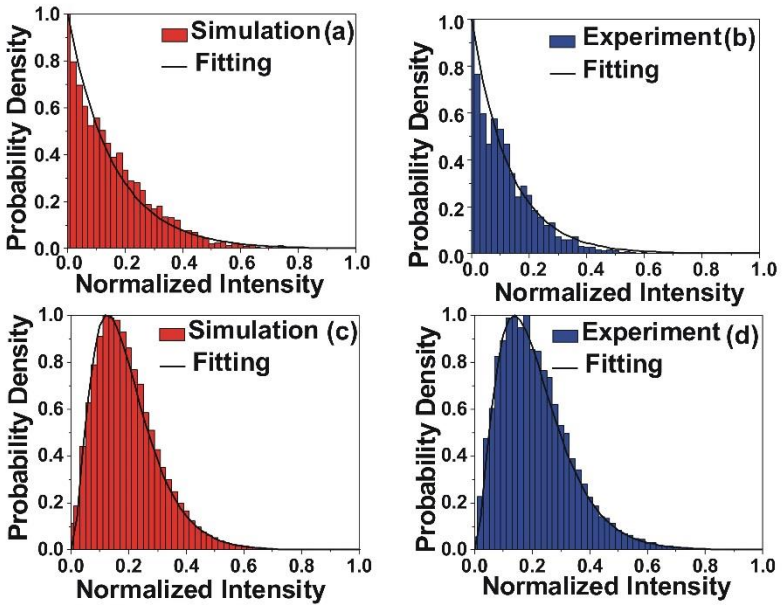

Figure 3.3 Intensity distribution of 50ns pulse with and input power of 10 mW: (a) simulation with polarization mismatch; (b) Experiment with coherent detection; (c) simulation with polarization match; (d) Experiment with polarization diversity detection.

Figure 3.4(a) and 3.4(b) show the normalized 100 consecutive Φ-OTDR traces with 50 ns pulse width by using the coherent detection and polarization diversity detection. The effective fiber length is from 180 m to 866m which corresponds to a fiber length of 686 m. The average intensity along the fiber length is labeled by the blue dash lines as indicated in figure 3.4. Different intensity along the fiber is caused by constructive and destructive interference. It is noted that the relative low intensity as shown in figure 3.4(a) is due to the polarization mismatch between the sensing arm and reference arm. The average intensity can be effectively enhanced along the fiber length by applying the PD method, as clearly illustrated in figure 3.4(b).

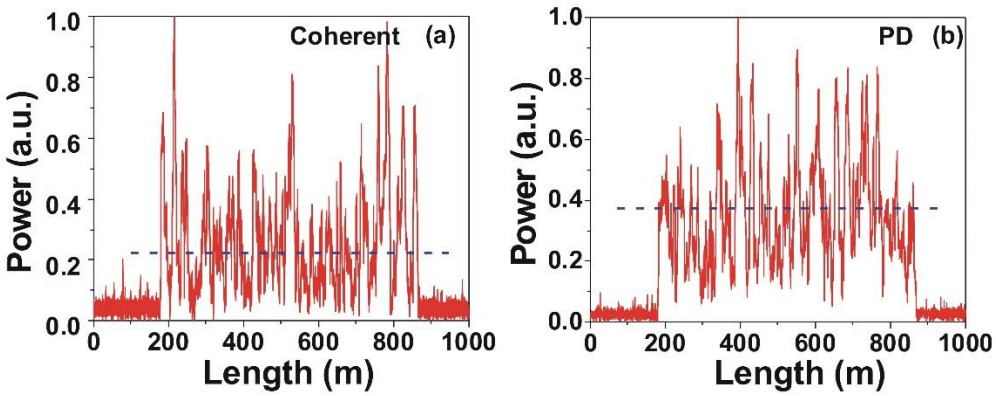

Figure 3.4 Normalized 100 superposition Φ-OTDR traces with 50ns pulse width: (a) coherent detection; (b): polarization diversity detection. Blue dash line: average intensity level of detected signal along the fiber length.

In Φ-OTDR system, usually SNR above 3dB is preferred for the sensing application. So the SNR of 3 dB is defined as a threshold to determine the ability of the sensor system. The detected SNR below 3 dBis considered as the noise signal. The percentage of SNR below threshold along the fiber length under the different pulse widths with same peak powers by using coherent detection and PD scheme is described in figure.3.5. The PD method effectively increase the probability of high SNR along the fiber length.

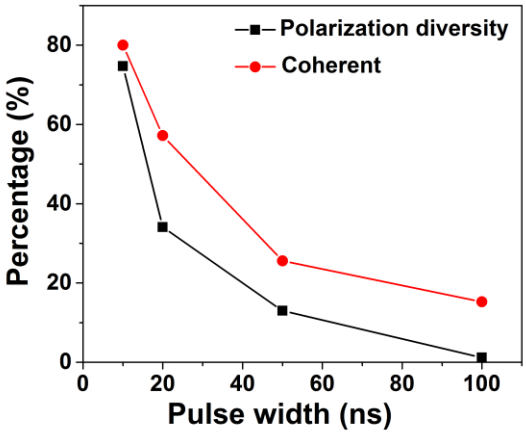

Figure 3.5 Percentage of detected SNR below 3dB threshold along the fiber length with different pulse width.

For vibration measurement based on the coherent detection, the PC is used to match the

polarization between two arms; however it needs the prior knowledge of the vibration location. Although the polarization mismatch can be eliminated at certain positions by adjusting the PC, this mismatch effect still exists at other positions along the sensing fiber. As a result, the external vibration is insensitive at those polarization mismatch positions resulting in low SNR signals at the vibration frequency. In the PD scheme, the signals at two orthogonal polarization states are detected independently so that the complementarity of the two signals can be guaranteed throughout the sensing fiber with high SNR of the Φ-OTDR system. The experiment was carried out by collecting 2000 consecutive traces using parameters of 50 ns pulse width, 10 mW input power, and 10 kHz repetition rate. Two events with vibration frequencies of 500 Hz and 800 Hz were detected simultaneously by using the coherent detection and polarization diversity detection, separately.

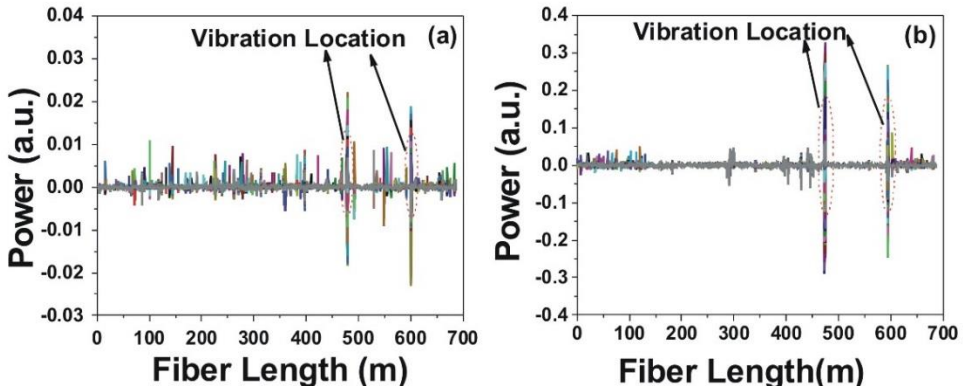

Figure 3.6 Vibration location information obtained by: (a) Coherent detection; (b) PD detection.

The vibration location information obtained by the coherent and PD detection after trace subtraction are shown in figure 3.6(a) and 3.6(b), respectively. The spikes occur at other non-vibration positions in the coherent detection are caused by the polarization fading induced trace-to-trace fluctuations. The vibration signals could submerge into the noise floor and show the misleading vibration locations. By eliminating the polarization mismatch induced fading noise, the

PD detection shows clear vibration signals with better SNR at both vibration locations compared with coherent detection.

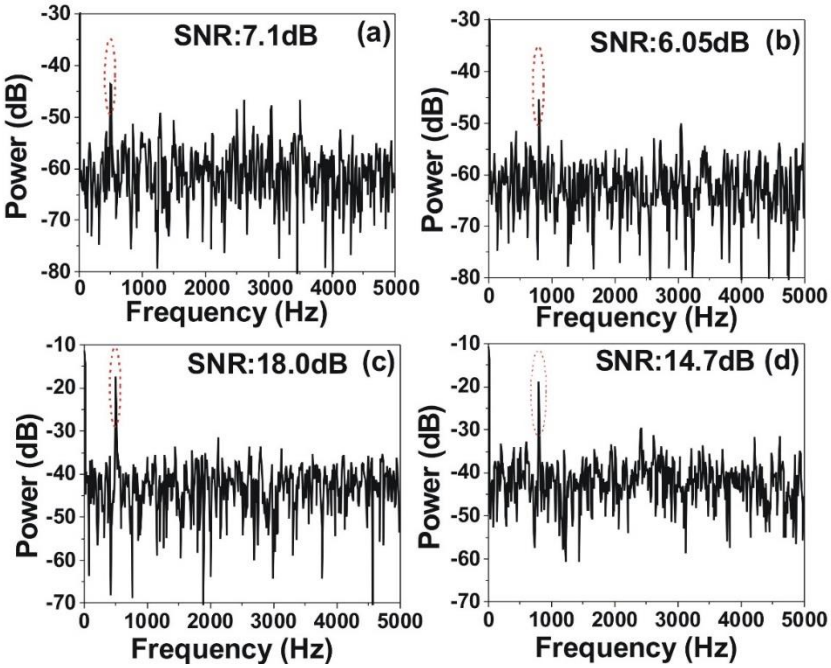

Figure 3.7 Power spectrum at two vibration locations obtained by coherent detection: (a) 500 Hz; (b) 800 Hz; PD detection: (c) 500 Hz; (d) 800 Hz.

Once both vibration events are located, the vibration frequency can be obtained by performing a FFT at each vibration location. Power spectra at two vibration locations based on coherent detection and PD detection are shown in figure 3.7. With the vibration frequencies of 500 Hz and 800 Hz, the SNR is improved by using PD detection for both events with enhancements of 10.9 dB and 8.65 dB, respectively. The polarization diversity scheme is theoretically effective to eliminate overall polarization fading caused by the polarization mismatch between the reference and sensing arms occurring in the coherent detection scheme. However, it has only a minor impact on the polarization of interfering signals between Rayleigh scattering centers within a pulse width because of the uncontrollable and chaotic polarization states of principal birefringence axes of the

reflectors [62]. Furthermore, although there is a greater probability that the polarization fading effect is completely eliminated at the two vibration positions, the PD method is still difficult to achieve good visibility over the whole sensing fiber simultaneously. In coherent detection by comparison, it would be more difficult to adjust the PC in the reference arm to different SOPs at both locations at the same time.

3.5 Conclusion

Distributed vibration sensing based on an Φ-OTDR system with polarization diversity detection has been proposed and demonstrated. Both theoretical and experimental results show that the proposed sensing system can achieve a more reliable vibration measurement result with high SNR signals compared with a traditional Φ-OTDR system. This technique eliminates the polarization mismatch between the sensing arm and reference arm at any given location of the sensing fiber making it is more suitable for the multi-events sensing applications.

Chapter 4

4 Piezoelectric Sinusoidal Vibration Measurement in Φ-OTDR

Vibration frequency measurement is easily achieved by using an Φ-OTDR system, but vibration amplitude measurement is difficult in an Φ-OTDR system due to the intensity fluctuation caused by the stochastic random characteristics of Rayleigh backscattering. In this chapter, an approach for measuring the piezoelectric sinusoidal vibration signals is theoretically and experimentally evaluated through analysis of the peak value of a FFT spectrum at the fundamental frequency and high-order harmonics, showing the validity of particular vibration modulation amplitude measurements within a certain range determined by the Bessel functions. A trace-to-trace correlation coefficient is introduced to quantify the system noise. High correlation coefficients varying from 0.82 to 0.94 are obtained in the 100 experiment measurements. The results show that the standard deviation of the amplitude measurement depends on system noise and also on the PZT vibration-induced extra phase and amplitude change. Section 4.1 is an introduction of Φ-OTDR for the different applications which have been demonstrated. Also, the motivation and challenge for measuring the amplitudes are addressed in this section. Section 4.2 presents the operation principle for measuring the piezoelectric sinusoidal vibration amplitudes. Section 4.3 shows the experimental details and discussion including the setup in 4.3.1 and results of both simulation and experiment in 4.3.2. The last section 4.4 is the conclusion.

4.1 Introduction

Estimating dynamic strain from vibration measurement is of great importance for many

applications. For example, distributed acoustic signal monitoring that is imperative in the field of oil and gas industry, structural health monitoring and non-destructive inspection of civil infrastructure, aircraft, vehicles and ships, earthquake and volcano surveillance in environmental monitoring, and so forth. Distributed optical fiber sensors that are mainly developed based on detection and analysis of backscattering light have attracted great attention over the past two decades since they provide many advantages over conventional optical sensors. Rayleigh scattering based OTDR was demonstrated for distributed measurement of fiber attenuation and locations of broken points [63]. Compared with the conventional OTDR, Φ-OTDR uses a highly coherent laser source which has a great potential in measuring small dynamic disturbances along the fiber with improved spatial resolution and sensitivity. The first Φ-OTDR system was reported by Taylor, et al. in 1993, to detect the weak refractive index change by injecting a narrow pulse [20]. The principle of e Φ-OTDR is based on interference between Rayleigh backscattered light from different scattering centers along the fiber within a pulse width. The relative phase changes of the electric fields coming from different scattering centers are sensitive to the vibration at a certain position. Due to its high sensitivity, Φ-OTDR was successfully demonstrated as an intrusion sensor with a simple direct detection scheme [21, 49]. Long range Φ-OTDR for intrusion sensing was also demonstrated with the assistance of Raman amplification [64]. Φ-OTDR was also demonstrated for vibration sensing by adopting heterodyne coherent detection [22]. The wavelet denoising method was introduced in Φ-OTDR to get a better performance with 50 cm spatial resolution [23]. A high frequency measurement was achieved by combining a Mach-Zehnder interferometer and an Φ-OTDR system [36].

The aforementioned works demonstrate the vibration frequency measurement ranging from Hz to kHz in terms of different applications. Although quantifying vibration is important in some

situations such as oil and gas exploration and crack damage detection in structural health monitoring, it was rarely discussed in literature. The phase demodulation method has been demonstrated in Φ-OTDR for dynamic strain measurement [65].However utilizing phase demodulation scheme is rather complex and its demodulation time is much longer than that required in the intensity monitoring technique. . In both phase and intensity measuring approaches, the challenge for dynamic strain measurements lies in the stochastic feature of the intensity fluctuation of Φ-OTDR traces, causing huge measurement uncertainty [66-68]. Thus minimizing intensity fluctuation by optimizing the Φ-OTDR system is necessary for precise dynamic strain measurements in Φ-OTDR.

4.2 Operation Principles

The Φ-OTDR can be used in vibration measurements by distinguishing changes in speckle-like traces of Rayleigh backscattered light. Vibration positions along the sensing fiber can be extracted by subtracting the trace sequences, and vibration frequency can be obtained by performing the FFT on the time domain waveform at each vibration location. External vibration will cause an extra phase change $\Delta\phi$ of the electric field of the detected signal. As cosine voltage is applied to a PZT cylinder where a section of the sensing fiber is wrapped around, the fiber length as well as the corresponding modal index and birefringence will experience periodic changes because of the piezoelectric effect of the piezo ceramics.

Rayleigh backscattered light in the single mode fiber can be modeled as a sequential series of spatially discrete reflectors. When a pulse of highly coherent light with central frequency of f_0 is injected into the sensing fiber, the electric field of the Rayleigh backscattered light at the fiber incident end at time t is the sum of the electric field of every Rayleigh scattering centers over half

of the pulse duration. Quasi-elastic Rayleigh scattering would not induce any time-dependent light frequency shift, provided that there is no temporal perturbation effect on fiber characteristics, which have the same resonant frequency as the laser frequency f_0 under a relative static state. The external vibration will cause an acceleration a, which can be written as $a = a_{\mathrm{m}} \cos(2\pi f_{\mathrm{vib}} t)$, where a_{m} is the maximum amplitude of the acceleration that is proportional to vibration modulation amplitude V_m.. A frequency shift Δf is consequently induced to its original resonant frequency f_0 so that the instantaneous resonant frequency $f(t)$ becomes [69],

$$f(t) = f_0 + \Delta f = f_0\left(1 + \Gamma a_m \cos(2\pi f_{\mathrm{vib}} t)\right), \tag{4.1}$$

where Γ is the acceleration-sensitivity vector, and it is set to be 1 as a typical case under small dynamic disturbances. The vibration induced phase can thus be expressed as

$$\phi_{\mathrm{vib}}(t) = 2\pi f_0 t + \left(f_0 \Gamma a_m / f_{\mathrm{vib}}\right)\sin(2\pi f_{\mathrm{vib}} t). \tag{4.2}$$

It is indicated that the phase change $\Delta\phi_{\mathrm{vib}}$ is proportional to $\Gamma V_m \sin(2\pi f_{\mathrm{vib}} t)$. So the vibration induced phase can be modified as:

$$\Delta\phi_{\mathrm{vib}}(t) = \Gamma V_m \sin(2\pi f_{\mathrm{vib}} t). \tag{4.3}$$

Then the intensity of the Φ-OTDR is an interference signal determined by the AC-term,

$$\begin{aligned} I &= 2\sum_{j=1}^{N-1}\sum_{k=j+1}^{N} {E_0}^2 r_j r_k e^{-2\alpha\left(z_j + z_k\right)} \cos\left(\Phi_0 + \Gamma V_m \sin(2\pi f_v t)\right) \\ &= 2\sum_{j=1}^{N-1}\sum_{k=j+1}^{N} {E_0}^2 r_j r_k e^{-2\alpha\left(z_j + z_k\right)} \cdot \begin{bmatrix} \cos\left(\Phi_0\right)\cos\left(\Gamma V_m \sin(2\pi f_v t)\right) \\ -\sin\left(\Phi_0\right)\sin\left(\Gamma V_m \sin(2\pi f_v t)\right) \end{bmatrix}, \end{aligned} \tag{4.4}$$

where E_0 is the initial electric field amplitude, r_j is reflectance of j-th reflector, a is an attenuation coefficient of the fiber, where $\Phi_0 = \Phi_{jk} + \delta\Phi_{jk}$, $\Phi_{jk} = \varphi_{\mathrm{j}} - \varphi_{\mathrm{k}}$ and $\delta\Phi_{jk}$ are respectively the phase difference and phase fluctuation difference between phases of two backscattered signals from j-th

and *k*-th reflectors, being part of a total number of *N* Rayleigh scattering centers existed over the spatial length of a short pulse. Then equation (4.4) can be further expanded by using an infinite series of Bessel functions,

$$
\begin{aligned}
I = & 2\sum_{j=1}^{N-1}\sum_{k=j+1}^{N} {E_0}^2 r_j r_k e^{-2\alpha\left(z_j+z_k\right)} \cdot \\
& \left\{ \begin{array}{l} \cos\left(\Phi_0\right)\left[J_0\left(\Gamma V_m\right) + 2\sum_{n=0}^{\infty} J_{2n}\left(\Gamma V_m\right)\cos(2n\cdot 2\pi f_{\text{vib}} t) \right] \\ -\sin\left(\Phi_0\right)\left[2\sum_{n=0}^{\infty} J_{2n+1}\left(\Gamma V_m\right)\sin\left((2n+1)\cdot 2\pi f_{\text{vib}} t\right) \right] \end{array} \right\} \\
= & 2\sum_{j=1}^{N-1}\sum_{k=j+1}^{N} {E_0}^2 r_j r_k e^{-2\alpha\left(z_j+z_k\right)} \cdot \\
& \left[\begin{array}{l} J_0(\Gamma V_m)\cos(\Phi_0) + \\ J_1(\Gamma V_m)\cos(\Phi_0 + 2\pi f_{\text{vib}} t) - J_1(\Gamma V_m)\cos(\Phi_0 - 2\pi f_{\text{vib}} t) + \\ J_2(\Gamma V_m)\cos(\Phi_0 + 2\pi\cdot 2 f_{\text{vib}} t) + J_2(\Gamma V_m)\cos(\Phi_0 - 2\pi\cdot 2 f_{\text{vib}} t) + \\ J_3(\Gamma V_m)\cos(\Phi_0 + 2\pi\cdot 3 f_{\text{vib}} t) - J_3(\Gamma V_m)\cos(\Phi_0 - 2\pi\cdot 3 f_{\text{vib}} t) + \ldots \end{array} \right]
\end{aligned}
\tag{4.5}
$$

From equation (4.4), the output intensity contains sinusoidal signal components with frequency f_v ,$2f_v$, $3f_v$, … and amplitudes, relative to $J_1(\Gamma V_m)$, $J_2(\Gamma V_m)$, $J_3(\Gamma V_m)$…. The first order Bessel function is used to monitor the vibration amplitude because the response of higher harmonics are weak due to the small amplitude induced by PZT. P_{peak} is the peak value of FFT spectrum of vibration frequency f_v. P_{peak} is proportional to the vibration modulation amplitude V_{m} in a certain range which is determined by the first order Bessel function, then V_{m} can be extracted from P_{peak} measurement.

4.3 Experiment details for measuring the sinusoidal vibration amplitudes in Φ-OTDR

4.3.1 Experimental setup

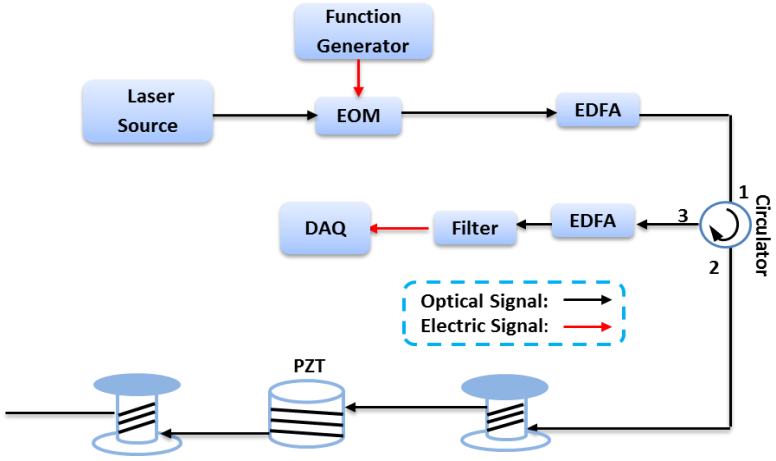

Figure 4.1 Experimental setup of the Φ-OTDR system for vibration modulation amplitude measurement.

The experimental setup of the Φ-OTDR for modulation amplitude measurement is shown in figure 4.1. An external cavity laser source operated at 1550 nm with narrow linewidth of 50 kHz was launched into an EOM controlled by a function generator with a repetition rate of 10 kHz and 50 ns pulse width. The high extinction ratio (>40dB) optical pulse is generated by the EOM. Also, the EOM bias is locked at the minimum point of transfer function by utilizing the bias controller with a feedback circuit. The modulated light was amplified by an EDFA and then the amplified pulse was sent into 690 m sensing fiber via a circulator. The Rayleigh backscattered signal is further amplified and the ASE is filtered out by a filter. Then the signal is detected by a photo-detector and processed by a DAQ. In the vibration measurement experiment, a section of the sensing fiber was wrapped around a cylindrical PZT. The piezoelectric transducer was driven by a function generator with output voltage ranging from 0 to 20 V and frequency ranging from Hz up to several kHz.

4.3.2 Results and discussion

A. Trace fluctuation characterization

It should be noted that irregular vibrations often occur in nature where they can be decomposed into a multitude of frequency components with unequal cycles. For instance, a piezoelectric transducer tube is usually used to generate a single-frequency vibration, while the dominant vibration can be practically disturbed by some undesirable effects such as an imperfect fiber wrapping process causing non-uniform vibration responses of the sensing fiber. As a matter of fact, these additional random vibration components besides the dominant one existing in a real test environment may cause an extra phase change of the electric field of the detected signal beyond the system noise, contributing to a certain degree of uncertainty in P_{peak}. To quantify the intensity fluctuation, thus an OTDR trace-to-trace correlation coefficient $R(M)$ is introduced to evaluate the level of the Φ-OTDR system instability as well as the standard deviation of measured P_{peak}, which is defined as:

$$R = \frac{1}{M-1}\sum_{i=1}^{M-1} r\left[k_i(z), k_{i+1}(z)\right] \tag{4.6}$$

where r is a correlation function between two adjacent traces, M is the total number of measurement traces, $k_{\text{i}}(z)$ is the normalized intensity of i-th trace at position z.

Figure 4.2 shows flow chart of the vibration measurement procedure by using Φ-OTDR. In simulation, phase φ of the individual reflector is a random quantity with a uniform probability distribution over the range of [0, 2π]. The phase fluctuation $\delta\Phi_{jk}$ has the uniform distribution on $F\cdot[0, 2\pi]$, where the coefficient F has a specific value in the range [0, 1] depending on the magnitude of the Φ-OTDR system noise. The phase fluctuation varies from trace to trace and contributes to the intensity fluctuation. The intensity of M Φ-OTDR traces at non-vibration

locations and vibration locations can be simulated based on equation (4.5). In experiment, M Φ-OTDR traces are acquired and stored in the computer. In order to analyze the system stability, trace-to-trace correlation function is performed at non-vibration locations. The wavelet denoising technique was adopted in the signal post-processing to reduce the random noise and then the vibration location can be identified by doing traces subtraction. After obtaining the vibration location, the FFT can be performed along traces at vibration location and P_{peak} will be recorded. The experiment will be carried out n times and the standard deviation of measured P_{peak} is also calculated to quantify the measurement uncertainty.

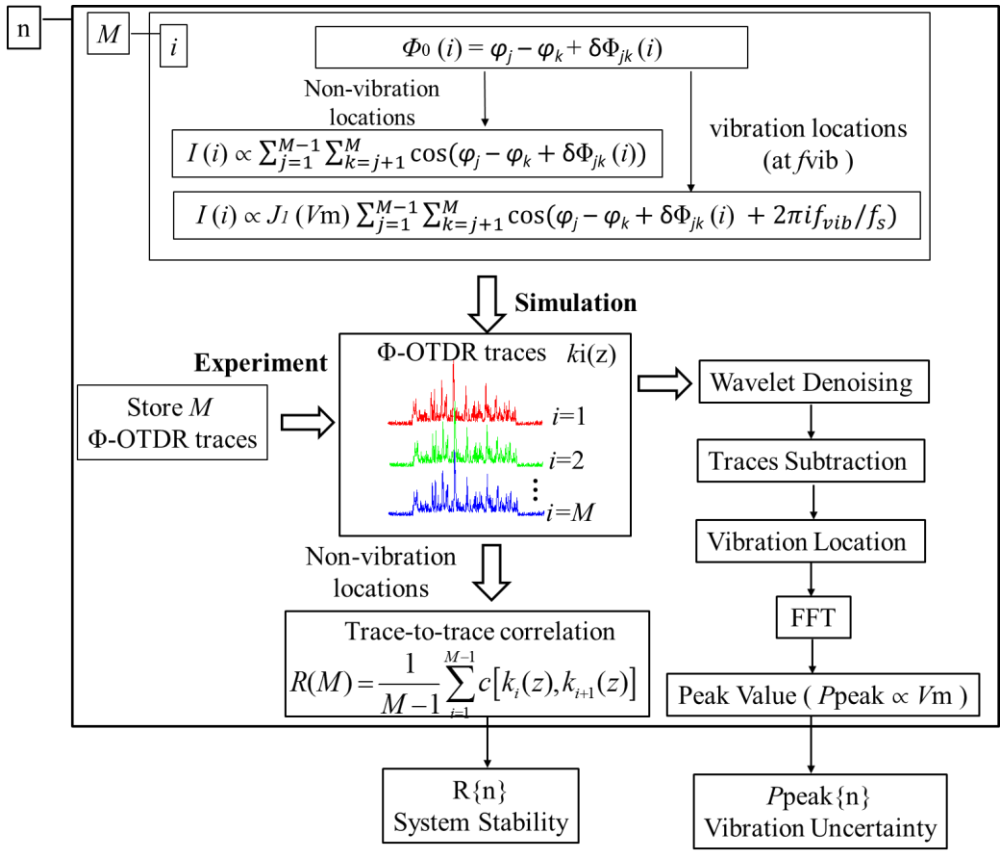

Figure 4.2 Flow chart of vibration measurement by using Φ-OTDR

Figure 4.3(a) shows the simulation result of trace-to-trace correlation coefficient under the different value of F. The trace-to-trace correlation coefficient can reach to 0.9928 when the F is

set as 0.001 and it decreases with increasing of F. 100 measurements are performed in the experiment and their average correlation coefficients at non vibration locations are calculated to test the system stability. The total number of traces M is 1000 in each measurement. The distribution of calculated correlation coefficients at non-vibration locations with the bin size of 0.01 is shown in figure 4.3(b). The experimental result shows that the correlation coefficient of measurements vary from 0.82 to 0.94. The high correlation coefficient shows that the system noise and fluctuation of measured Φ-OTDR traces is small. Figure 4.3(c) shows the experimental result of three traces in one measurement. The correlation coefficient of 0.9 is obtained in this measurement by using 1000 traces.

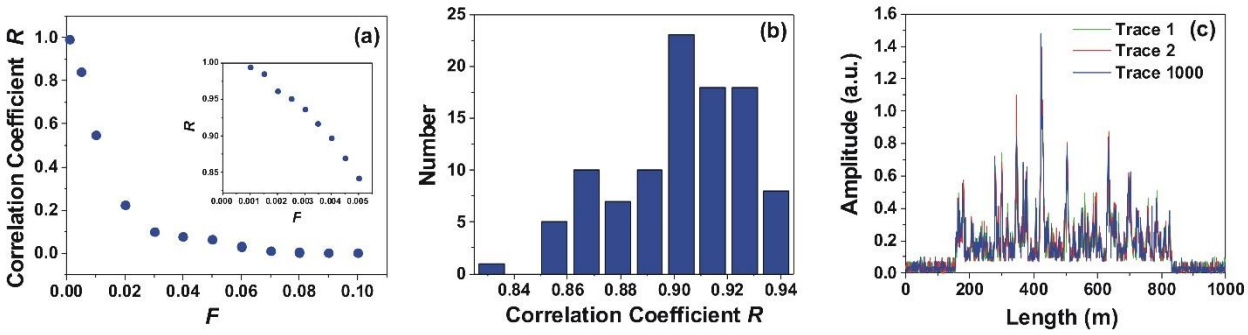

Figure 4.3 (a) The distributed correlation coefficient at non-vibration locations obtained with 100 measurements in the experiment. (b): The simulation result of correlation coefficient with varied fluctuation range F; (c): The experiment result of three Φ-OTDR traces

B. Vibration measurements

Figure 4.4(a) exhibits the first order and second order Bessel function, J_1 and J_2, respectively. The data points of A, B, and C on the curve of the first order Bessel function correspond to figures 4.4(b), 4.4(c), and 4.4(d) which are simulated power spectra with V_m = 0.25, 1, and 2. Since the output of any order Bessel functions would change with different V_m, the vibration modulation amplitude can thus be acquired by observing P_{peak} of corresponding frequency in the power spectra.

In figure 4.4(b), there is one peak at the vibration frequency f_{vib} = 500 Hz under the modulation amplitude of 0.25. According to equation (4.5), harmonics of higher orders in terms of Bessel functions remain and become more and more noticeable for larger V_m values. Another peak at 2fvib in figure 4.4(c) and even three other peaks at harmonic frequencies in figure 4.4(d) appear in the power spectra when V_m was further increased. The amplitudes of these peaks are determined by the magnitude of the second order and third order Bessel functions.

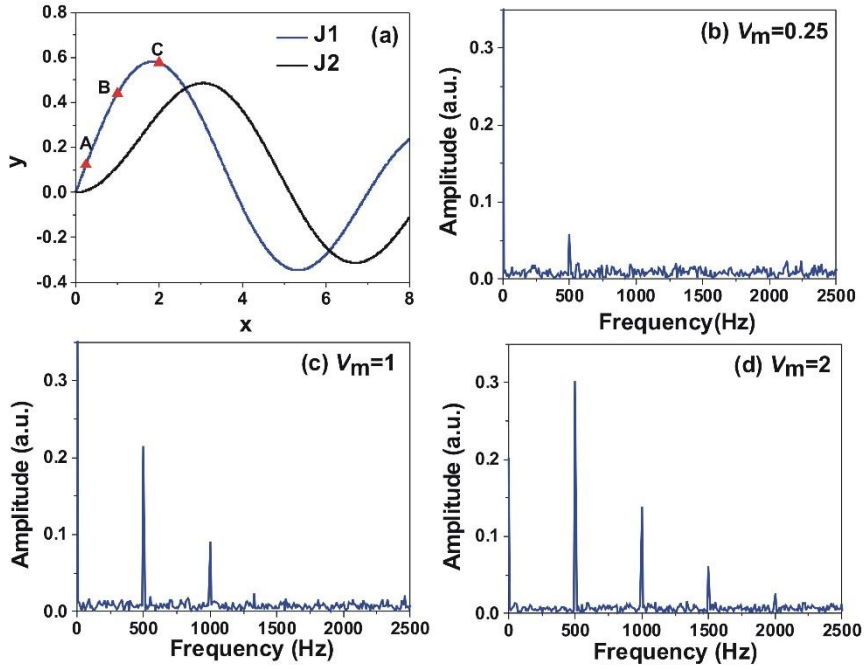

Figure 4.4 (a) The first order and second order Bessel functions. A, B, C corresponds to figures. 4.4(b), 4.4(c), 4.4(d), respectively. Simulation results of power spectra under different modulation amplitudes: (b) V_m = 0.25; (c) V_m = 1; (d) V_m = 2.

The above theoretical and simulation analysis indicates that the detection of V_m becomes available by monitoring relative peak amplitudes at the fundamental frequency and high-order harmonics, however, this work only demonstrates the case that the first order Bessel function plays a dominant role. The wavelet denoising technique was adopted in the signal post-processing to

reduce the system noise and enhance spatial resolution, and thus the vibrating location detection accuracy was greatly improved. The 500 Hz vibration event was identified at 490 m as shown in Figure 4.5(a). Figures 4.5(b), 4.5(c), and 4.5(d) show the measured power spectra with different vibration modulation amplitudes of V_m = 1.8V, 3V, and 4V.

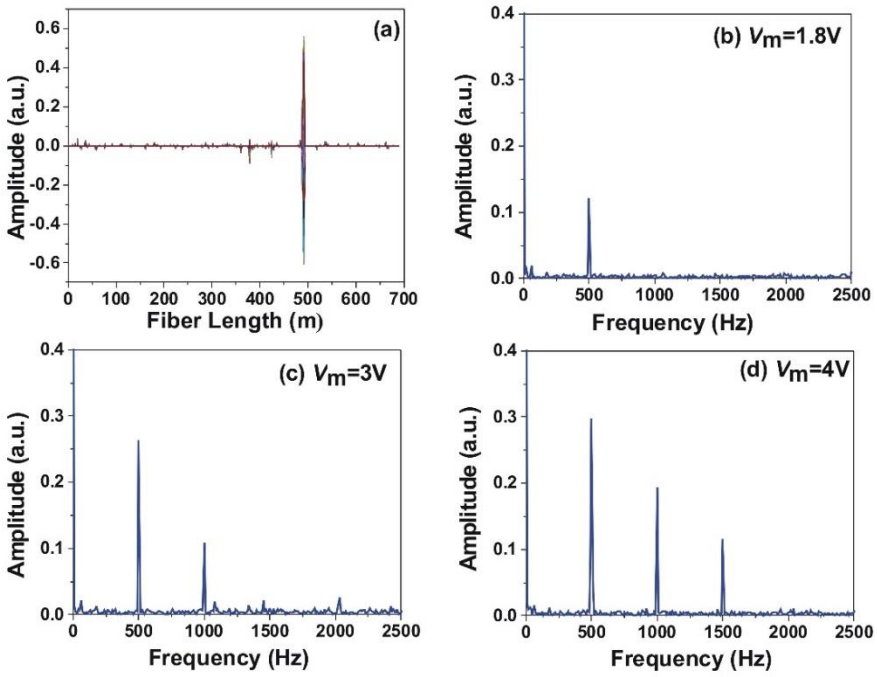

Figure 4.5 (a) vibration location information. Experiment results of power spectra under different modulation amplitudes :(b) V_m = 1.8V; (c) V_m = 3V; (d) V_m = 4V.

In simulation, the vibration signal is modeled as the perfect sinusoidal signal and thus the standard deviation of measured peak value depends only on the system noises which can be characterized by the correlation coefficient R. Figure 4.6(a) shows the simulation result of standard deviation of P_{peak} with varying of correlation coefficients under V_m = 0.25. Figures 4.6(b) and 4.6(c) show the simulation and experimental results of standard deviation of P_{peak} measurements with different number of traces under the amplitude V_m = 0.25 and V_m = 2.2V. The blue dots and red dots in figure 4.6(a) are obtained by using F= 0.004 and F= 0.055 which corresponding to

correlation coefficient R = 0.9 and 0.03, respectively. All results are calculated with 100 measurement samples. Although the average correlation coefficient in the experiment results is around 0.9, the standard deviation of measured peak value in experiment result is much larger than that of simulation result. The standard deviation is comparable with the simulation result under the correlation coefficient of 0.03. The larger standard deviation in the experiment is caused by the PZT vibration induced extra phase and amplitude change, resulting in a reduction of correlation coefficient. Also from both figures 4.6(b) and 4.6(c), the standard deviation becomes smaller when more traces is used for the spectrum analysis. It is because that the average random noise is approaching the same in each measurement when more traces are used. Thus, 1000 traces are selected in the experiment to get small measurement uncertainty and save the measurement time.

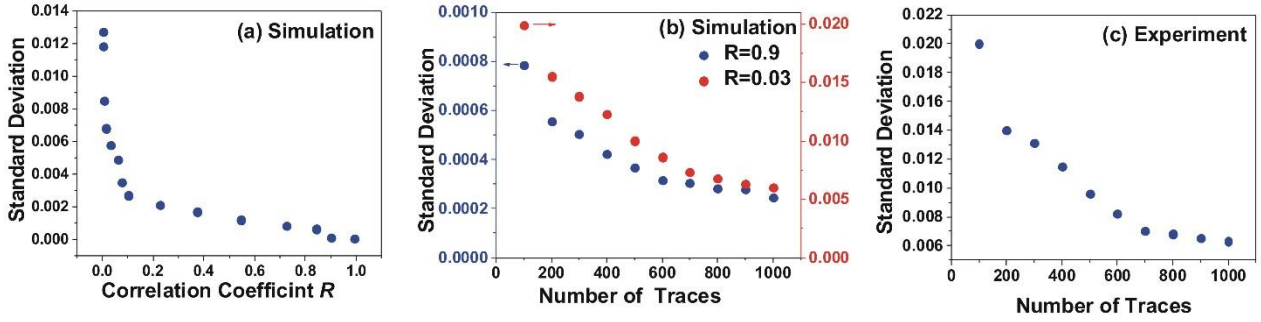

Figure 4.6 (a) Simulation result of standard deviation of P_{peak} with varying of correlation coefficient. The standard deviation of P_{peak} with number of traces: (b) simulation: V_m= 0.25; and (c) experiment: V_m= 2.2V.

Figures 4.7 (a) and 4.7 (b) show the simulation results and the experiment result of measurement P_{peak} with different applied modulation amplitudes. F is set as 0.055 and the correlation coefficient is 0.05 in the simulation to match the experiment result. Both simulation and experiment were obtained by performing FFT with 1000 traces and replicated 100 times to guarantee reliable and repeatable results. The modulation amplitude can be statistically extracted from the average value of P_{peak}. The experimental results show that the Φ-OTDR system has a

high stability and low phase fluctuation since high correlation coefficients and relative small vibration amplitude measurement uncertainty.

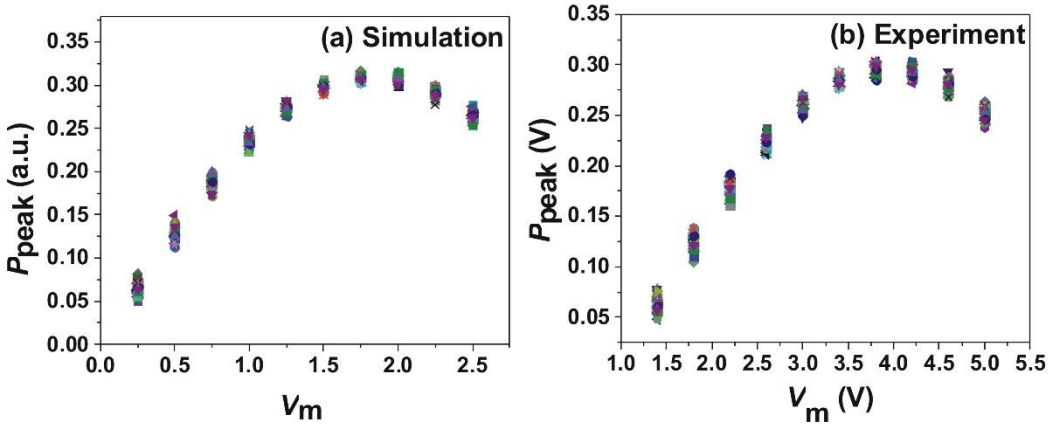

Figure 4.7 The change of *P*peak with different modulation amplitudes V_m: (a) simulation (b) experiment.

4.4 Conclusion

In conclusion, an approach to measure the vibration amplitude is theoretically proposed and experimentally demonstrated. The PZT vibration modulation amplitude has been characterized by monitoring the peak value in the power spectra obtained by using the FFT. The measurement range is determined by the increased range of first order Bessel function. The trace-to-trace correlation coefficient is also introduced to analyze the system stability and the measurement uncertainty. The experimental results demonstrate a good agreement with the simulation results.

Chapter 5

5 Performance enhancement in Φ-OTDR based on high extinction ratio optical pulse generation

In an Φ-OTDR system, the extinction ratio (ER) of an optical pulse generated by an EOM is finite and the CW leakage light could deteriorate the detected signal. The SNR of an Φ-OTDR sensor system could be increased by utilizing a high extinction ratio optical pulse. In this chapter, the effect of finite ER in an Φ-OTDR is theoretically analyzed and experimentally proved. To improve the ER of an optical pulse, two approaches for generating the high ER optical pulse are introduced. Synchronizing the dual EOMs and applying the nonlinear loop mirror are demonstrated in detail for high ER pulse generation. Vibration measurement with a sensing range of 1.8 km and 0.5 m spatial resolution has been achieved based on a dual EOMs setup. The sensing range of 8.4 km and spatial resolution of 2 m has been demonstrated based on nonlinear loop mirror. Section 5.1 gives an introduction of the background which illustrates the motivation of this work. The two approaches of dual EOMs and nonlinear loop mirror are demonstrated in section 5.2 and 5.3 respectively including the details of the theoretical analysis and experiment work. Section 5.3 is the conclusion.

5.1 Introduction

Since Φ-OTDR system was proposed by Taylor for distributed intrusion sensing in 1993 [20], it has attracted many attentions and found its great potential in distributed sensing applications due to its high sensitivity, long sensing range and good spatial resolution. The Φ-OTDR system utilizes the highly coherent laser whose coherent length is much longer than the fiber length. The laser is

modulated to generate optical pulses which are sent into the fiber, and then the Rayleigh backscattered light from different backscattering centers within the pulse width could interfere each other and form speckle patterns in Φ-OTDR traces. Generally, the optical pulses are modulated by an EOM. The bias voltage of EOM does not stay constant which will affect the performance of sensor system. Although the EOM bias [34] could be locked at the working point, the stable ER of commercial EOMs are generally 30~40dB. In Φ-OTDR system, the optical pulses need to be amplified to detect the Rayleigh backscattering before entering into the fiber but the CW component of optical pulse are also amplified. Thus the Rayleigh backscattered light induced by the strong CW component would interfere with the pulse portion, result in reduction of the SNR of sensor system. This problem becomes more serious for the long range and high spatial resolution sensing application because SNR is much lower in these cases. The trace fluctuation caused by the leakage light is more obvious which makes it difficult to detect the external vibration. Therefore, it is desired to enhance the extinction ratio of optical pulse in Φ-OTDR system, especially for long range and high spatial resolution sensing.

5.2 High extinction ratio optical pulse generation with dual cascaded electro-optical modulators

5.2.1 Effect of finite extinction ratio in Φ-OTDR

Figure 5.1 Optical pulse with finite extinction ratio

In Φ-OTDR system, EOM is used to convert CW light into the short optical pulse. However, the ER of generated pulse is finite and the CW leakage is induced in addition to the pulse. Figure 5.1 shows the optical pulse with the finite ER. P_p and P_{cw} are the peak power and CW leakage power of incident light. The power of Rayleigh backscattered light generated by pulse and CW leakage, denoted by P_{bp} and P_{bcw} are expressed as:

$$\begin{aligned} P_{bp}(z) &= P_p \alpha_R \frac{cT_p}{2n} e^{-2\alpha z} \\ P_{bcw} &= 2\alpha_R \int_0^L P_{cw} e^{-2\alpha z} dz = \frac{P_{cw}\alpha_R (1-e^{-2\alpha L})}{\alpha} \end{aligned} \tag{5.1}$$

where T_p is the pulse duration, α is the attenuation coefficient of single mode fiber, α_R is the Rayleigh backscattering coefficient, n is the refractive index of optical fiber and L is the fiber length. From equation (5.1), the pulse peak power of backscattered light behaves in an exponential decay form along the fiber length and the CW portion is constant along the fiber. Because the highly coherent laser used in the Φ-OTDR system, the backscattered light from CW part could interfere with the pulse part and the power of interference light, $P_{int}(z)$ is:

$$P_{int}(z) = 2\sqrt{P_{bp}(z)P_{bcw}} = 2\sqrt{P_p \alpha_R \frac{cT_p}{2n} e^{-2\alpha z} \frac{P_{cw}\alpha_R (1-e^{-2\alpha L})}{\alpha}} \tag{5.2}$$

In an ideal case of infinite ER, both terms of P_{bcw} and P_{int} would vanish in the system. But in the real case, these terms are considered as the noise sources of the sensor system. Compared with P_{int}, P_{bcw} is small and could be ignored here. The SNR by only considering the intra-band noise would be:

$$SNR(z) = \frac{P_{bp}}{P_{int}} = \frac{P_p \alpha_R \frac{cT_p}{2n} e^{-2\alpha z}}{2\sqrt{P_p \alpha_R \frac{cT_p}{2n} e^{-2\alpha z} \frac{P_{cw}\alpha_R (1-e^{-2\alpha L})}{\alpha}}} = \sqrt{ER}\sqrt{\frac{c\alpha T_p e^{-2\alpha z}}{8n(1-e^{-2\alpha l})}} \tag{5.3}$$

where $ER=P_p/P_{cw}$. From equation (5.3), the SNR is proportional to the square root of ER and also decreases with the longer fiber length and narrower pulse duration used in the system. Thus, the high ER optical pulse is essential for the long range and high spatial resolution measurement of Φ-OTDR.

5.2.2 Experiment setup

The setup configuration of Φ-OTDR based on the high ER pulse generation is shown in figure 5.2. The high ER pulse generation is realized by synchronizing two cascaded EOMs. The laser source is a highly coherent fiber laser with 3 kHz linewidth and the EOM1 and EOM2 with ER of 30 dB and 40 dB are used in the experiment. The bias voltages of both EOMs are locked at the minimum point of transfer function by the feedback circuit. The amplified optical pulse is sent into the fiber under test through a circulator and the Rayleigh backscattered light is further amplified by an EDFA 2. The ASE noise is filtered out by a filter and the backscattered light is directly detected by a photodetector. In the experiment, EOM1 generates an optical pulse with a 50 ns pulse width and the pulse width of EOM2 is varied for the different experimental tests. To synchronize two EOMs, the pulse delay is adjusted properly through the pulse generator to make them overlap each other. In vibration sensing experiments, the PZT is acted as a vibration source which is driven by a function generator. The sampling rate is set at 250 M/s to obtain the Φ-OTDR traces. The wavelet denoising method is applied in the post signal processing to eliminate the random noise of trace fluctuation and to improve the SNR.

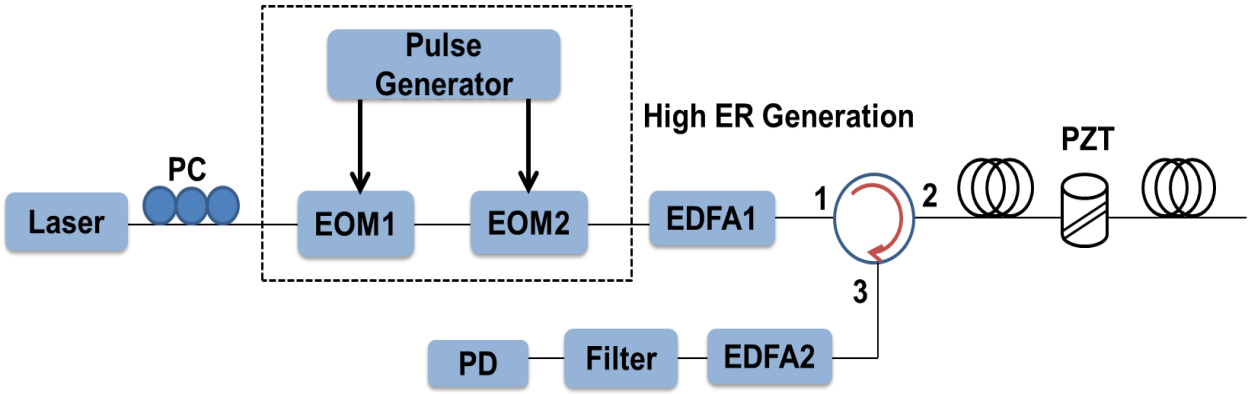

Figure 5.2 The schematic of Φ-OTDR with two cascaded EOMs

5.2.3 Experimental results and discussion

Figures 5.3(a), 5.3 (b) and 5.3 (c) illustrate the three optical pulses generated by using EOM1 with ER of 30 dB, EOM2 with ER of 40 dB and cascaded EOMs. The CW light of optical pulse is effectively suppressed in cascaded EOMs case. To verify the influence of leakage light on the SNR of Φ-OTDR system, the Φ-OTDR experiments are performed in above three cases. Figures 5.4 (a), 5.4(b) and 5.4(c) show two consecutive Φ-OTDR traces obtained by EOM1, EOM2 and cascaded two EOMs, respectively. The results are obtained by using a pulse width of 10ns and fiber length of 8.4km. The ripples occurred between two Φ-OTDR traces in the figures 5.4(a) and 5.4(b) are the interference signal caused by the leakage light. The interference signal induced by the leakage light becomes more visible in the case of 30 dB ER and it almost disappears in the case of dual cascaded EOMs. Due to the strong trace fluctuation induced by the CW interference, the Φ-OTDR system with lower ER is more difficult to measure the vibration. But in the dual EOMs setup, the optical traces become much more stable even for a very narrow pulse width and long fiber length. Thus, the performance of Phase-OTDR is improved effectively by the use of dual EOMs.

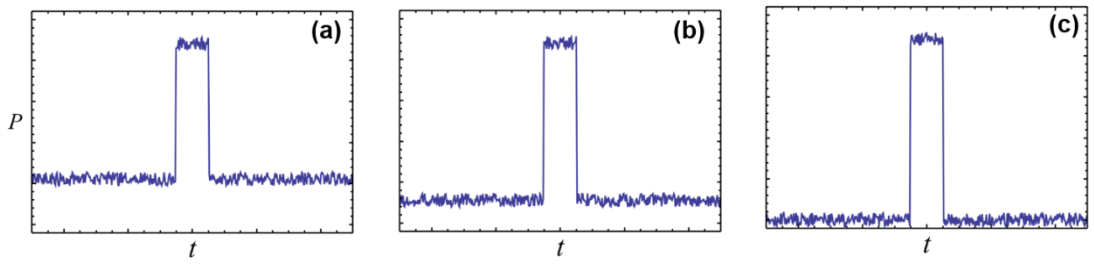

Figure 5.3 Optical pulses generated by: (a) EOM1; (b) EOM2; (c) cascaded EOMs

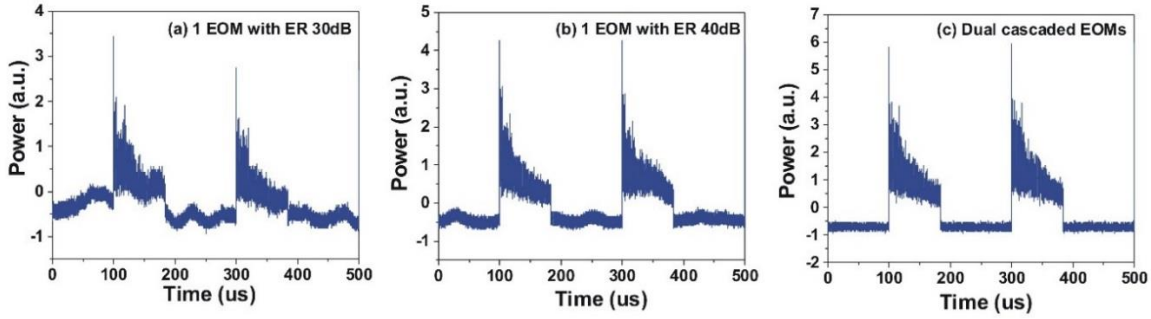

Figure 5.4 The two consecutive Φ-OTDR traces obtained by (a) EOM1 with 30dB; (b) EOM1 with 40dB; (c) Dual cascaded EOMs.

500 consecutive traces are collected in the experiment by using dual EOMs setup. The two vibration experiments are performed with the fiber lengths of 1.8 km and 8.4 km, respectively. The first experiment is conducted by using 1.8 km fiber and a pulse width of 5 ns. The repetition rate in this case is 10 kHz. The 40 cm length fiber was wrapped around the PZT tube for the high spatial resolution measurement. Figures 5.5(a) and 5.5(b) show the obtained vibration location information after traces subtraction. The spatial resolution of 0.5 m is achieved which is clearly shown in figure 5.5 (b). Figure 5.5(c) show the vibration frequency spectrum obtained by performing the FFT at vibration location. From figure 5.5 (a), the vibration location is obtained with a very high SNR of about 40 dB.

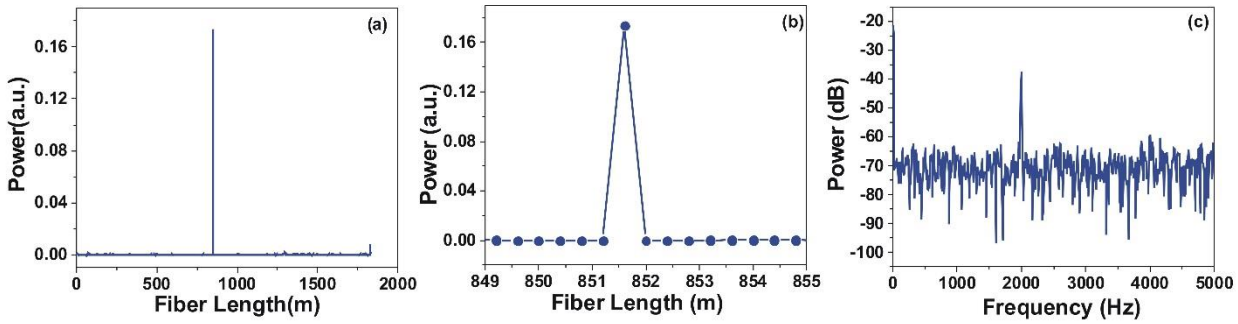

Figure 5.5 (a) vibration location obtained with 1.8km fiber (b) The zoom of (a) around the vibration location (c) power spectrum of vibration signal

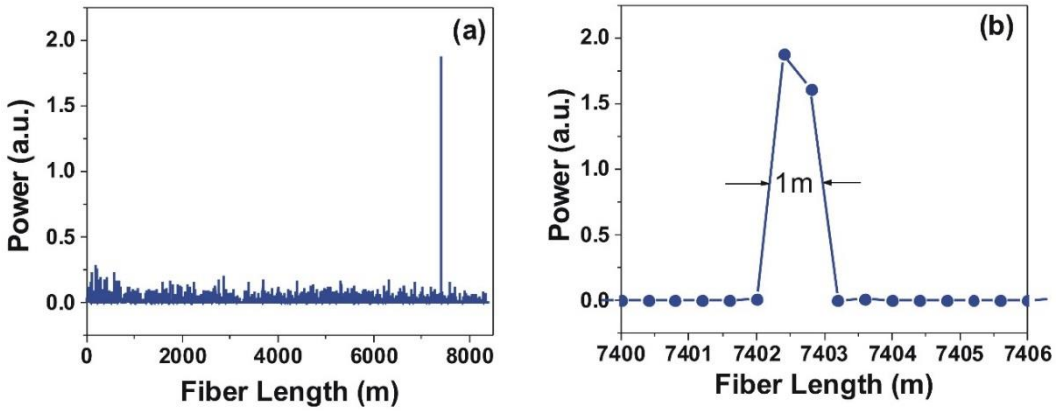

Figure 5.6 (a): Vibration position obtained with 8.4 km fiber (b) the zoom in graph of (a) around the vibration location

To test the system's performance for long sensing range measurement, we extend the fiber length to 8.4km. In this case, the pulse width is increased to 10ns because the SNR at rear end of fiber is too low to obtain the vibration information. Then the vibration location is shown in Fig.5.6 (a) with 8.4 km sensing range. Fig.5.6 (a) is zoomed in around the vibration position to clearly observe the vibration spatial information, which is shown in Fig.5.6 (b). The half width of the peak illustrates the spatial resolution is 1m corresponding to the 10 ns pulse width used in the experiment. The SNR of vibration signal is 23 dB in this case. Compared to the result obtained in 1.8 km, the

SNR is decreased because the trace to trace fluctuation is relatively larger for longer sensing fiber. The laser frequency drift could contribute to the intensity fluctuation since longer time measurement is required for longer fiber.

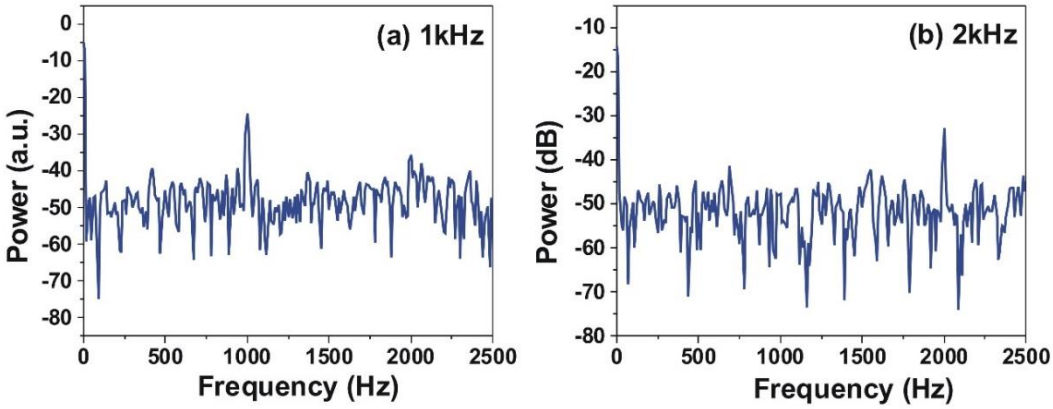

Figure 5.7 Power spectrum of detected vibration by doing the FFT (a): 1 kHz; (b) 2 kHz

The vibration frequency can be obtained by performing the FFT along the measured traces at vibration location. Two different frequencies of 1 kHz and 2 kHz are measured in the experiment and their power spectrum are shown in figures 5.7 (a) and 5.7 (b), respectively. The maximum frequency response here is limited to 2.5 kHz due to the 5 kHz repetition rate used in the experiment. The dual EOMs setup successfully enhances the ER of the optical pulses to above 60 dB and reduces the intra-band noise in the Φ-OTDR significantly. Using the high ER pulse generation, the system performance is enhanced and the vibration measurements are achieved with 0.5 m spatial resolution for 1.8 km sensing range. In addition, vibration sensing performance of 8.4 km fiber and 1m spatial resolution is achieved without any distributed amplification scheme.

5.3 High extinction ratio optical pulse generation with nonlinear optical fiber loop mirror

5.3.1 Introduction of nonlinear optical fiber loop mirror

In section 5.2, the dual EOMs setup is demonstrated for high extinction ratio optical pulse generation. One drawback of this dual EOMs scheme is that resulting ER is strongly dependent on ER of individual EOM used in the experiment. The EOM with high ER is usually expensive and it is difficult for practical use. Also, the insertion loss is large in this setup and two pulse generators are required. Besides the dual EOMs scheme, the nonlinear optical fiber loop mirror (NOLM) can also achieve the generation of high ER optical pulse. NOLMs have been extensively studied for various applications such as optical switching [70], demultiplexing [71], and passive mode locking [72] etc. NLOMs can be used as the saturable absorber, which allows very low transmission at low input power, whereas it becomes completely transparent for some higher value of the input power. NLOM has been reported in the Brillouin optical time domain analysis to enhance the ER of an optical pulse [73], however it has not been applied in the Φ-OTDR for vibration sensing yet.

5.3.2 Principle of nonlinear optical fiber loop mirror

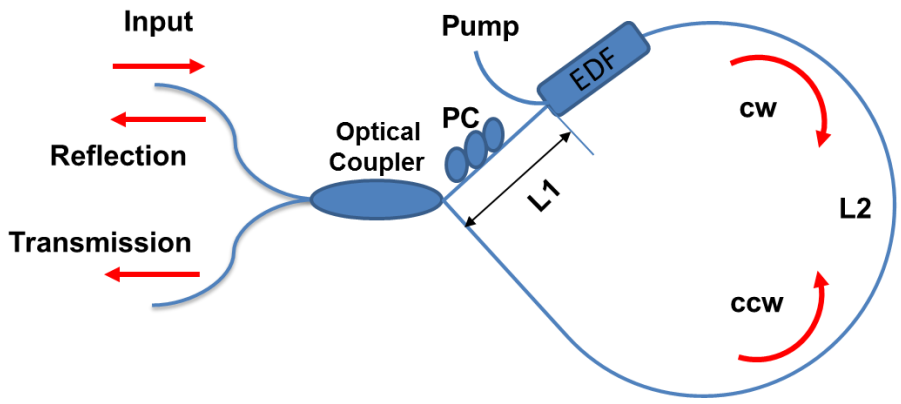

Figure 5.8 Schematic of nonlinear optical fiber loop mirror

The configuration of nonlinear amplifying optical fiber loop mirror is shown in figure 5.8. The NOLM consists of an optical coupler, the polarization controller, an erbium doped fiber (EDF) as a gain and a section of fiber. Before discussing the operational principle of nonlinear fiber loop mirror, the mathematical analysis of fiber loop mirror is presented. The schematic of fiber loop mirror is similar with the configuration in figure 5.8 except without the EDF gain. The reflection *R* and transmission *T* function of a linear loop at two ports of optical coupler can be expressed as:

$$\begin{aligned} R &= 4\varepsilon(1-\varepsilon) \\ T &= 1-4\varepsilon(1-\varepsilon) \end{aligned} \tag{5.4}$$

where ε is the coupling ratio of optical coupler. Thus the use of 50:50 optical coupler (ε=0.5) can obtain the 100% reflection and 0% transmission. However with a gain medium in the fiber loop, the nonlinear phase shift can be induced by asymmetrical amplification process of clockwise light and counter-clockwise light. The transmission and reflection of optical power is then determined by this nonlinear phase shift which is related to the input power, the gain of EDF and the fiber length. In the mathematic formulation, the electrical field of input light is:

$$E_{in} = E_0 \exp\left[j(wt + \phi_0) \right] \tag{5.5}$$

where E_0 is the amplitude of electrical field of input light and ϕ_0 is the initial phase of light. The optical signal goes through the coupler and splits into the clockwise and counter-clockwise directions and then combined at both the reflection and transmission ends. The electrical filed of clockwise and counter-clockwise signal at transmission end are:

$$\begin{aligned} E_{\mathrm{cw}} &= (1-\varepsilon)\sqrt{g}E_0 \exp\left[j(wt + \phi_0 + \phi_1 + \phi_{\mathrm{Lcw}} + \phi_{\mathrm{hcw}}) \right] \\ E_{\mathrm{ccw}} &= \varepsilon\sqrt{g}E_0 \exp\left[j(wt + \phi_0 + \phi_1 + \pi + \phi_{\mathrm{hccw}} + \phi_{\mathrm{Lccw}}) \right] \end{aligned} \tag{5.6}$$

where g is the gain factor, ϕ_1 is the linear phase after traveling through the fiber loop. ϕ_{Lcw} and

ϕ_{Lccw} are the nonlinear phase of the clockwise light and counter-clockwise light traveling before the EDF fiber, ϕ_{hcw} and ϕ_{hccw} are the nonlinear phase of the clockwise light and counter-clockwise light traveling after the EDF fiber, which can be written as:

$$\begin{aligned}
\phi_{\text{Lcw}} &= \Upsilon(1-\varepsilon)E_0^2 L_1 \\
\phi_{\text{Lccw}} &= \Upsilon\varepsilon E_0^2 L_2 \\
\phi_{\text{hcw}} &= \Upsilon(1-\varepsilon)E_0^2 g L_2 \\
\phi_{\text{hccw}} &= \Upsilon\varepsilon E_0^2 g E_0^2 L_1
\end{aligned} \tag{5.7}$$

Thus the transmission function can be expressed as:

$$T = (1-\varepsilon)^2 g + \varepsilon^2 g - 2(1-\varepsilon)\varepsilon g \cos\left[\Upsilon(1-\varepsilon-\varepsilon g)E_0^2 L_1 + \Upsilon(g-\varepsilon g-\varepsilon)E_0^2 L_2\right] \tag{5.8}$$

If ε=0.5 where the 50:50 coupler is used, the transmission function reduces to:

$$\begin{aligned}
T &= g/2\left(1-\cos\left[\Upsilon P_0(g/2-1/2)(L_2-L_1)\right]\right) \\
&\approx g/2\left(1-\cos\left[\Upsilon P_0(g/2-1/2)L\right]\right)
\end{aligned} \tag{5.9}$$

Thus, the transmission function depends on the input power P_0, gain factor g, and the fiber length L used in the loop. Given a fixed L and g, the nonlinear fiber loop mirror can act as a switch which only allows the high power to transmit. If the input signal is a pulse, the NOLM can be optimized so that the CW leakage light is reflected and only the pulse peak portion can transmit. This operation can significantly improve the extinction ratio of the optical pulse. Figure 5.9 shows the simulation result of transmission function with different input power P_0 under the gain of 10, 32 and 100. The fiber nonlinearities coefficient γ is 2/Wkm and the fiber length is 500m in the simulation. The maximum transmission occurred in the lower input power under higher gain. Also, for a given input power, the transmission is increased when the gain becomes larger and the output power is amplified at the transmission end of NOLM.

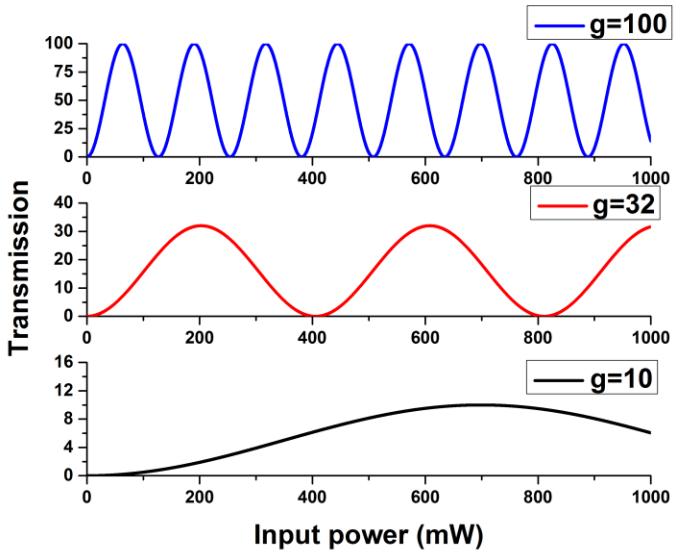

Figure 5.9 The transmission function of NOLM with different power under the g=10, 32 and 100.

The CW light of optical pulse generated by EOM is usually in the order of micro watts which would be easily reflected. The pulse peak power is 10 mW in our case and it could be transmitted totally by properly choosing the gain. The simulation result of transmission function with different gain under the input power of 10mW is shown in figure 5.10. The optical pulse is transmitted (T=1) without amplification when g is about 56. In the Φ-OTDR system, the optical pulse generated by EOM need to be amplified and the required peak power is usually between tens mW and hundreds mW in terms of different applications. Thus the EDF fiber should provide a gain of 100 which is 10 dB at least. As long as the optical pulse peak portion starts to switch and the desired peak power is obtained, the high ER of optical pulse is generated without further amplification required. Although the CW could be suppressed by adjusting the PC, ER is limited by the Rayleigh scattering generated in the loop. The use of short fiber could mitigate effects caused by Rayleigh scattering.

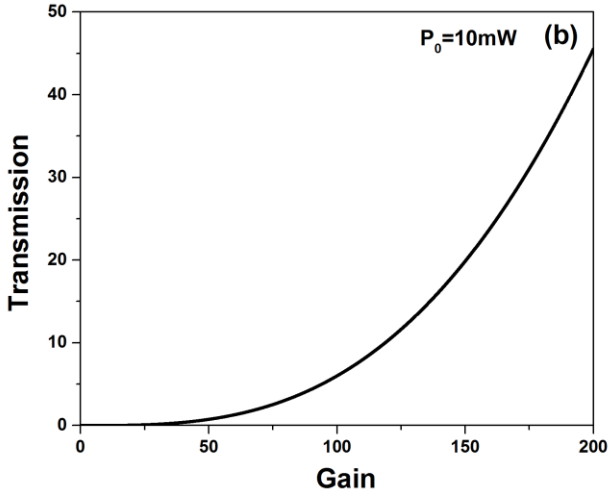

Figure 5.10 The transmission function of NOLM with different gain under the input power of 10 mW.

5.3.3 Experimental setup

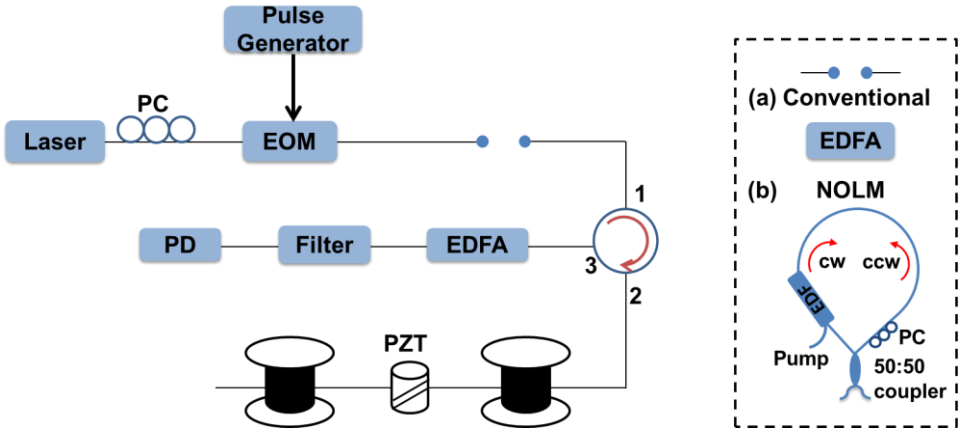

Figure 5.11 The Φ-OTDR sensor system: (a): conventional setup; (b): NOLM.

The configuration of Φ-OTDR sensor systems based on the conventional setup and NOLM are shown in figures 5.11(a) and 5.11(b), respectively. The laser used is a highly coherent fiber laser with a linewidth of 3 kHz. In the conventional Φ-OTDR setup, the commercial EDFA is used to amplify the very weak pulse generated by EOM. By replacing the EDFA with an amplifying

NOLM, the optical pulse is not only amplified but the CW leakage light is also effectively suppressed. An EDF fiber with 1.2 m length is positioned at the end of the loop and the optical coupler has a splitting ratio of 50:50. The 980 pump laser is coupled to the EDF fiber through a WDM to provide a sufficient gain. After the high ER optical pulse is obtained, it is sent into the fiber via a circulator. The Rayleigh backscattered light then is further amplified and the ASE noise is filtered out by the filter and detected by the photo-detector (PD).

5.3.4 **Experimental results and discussion**

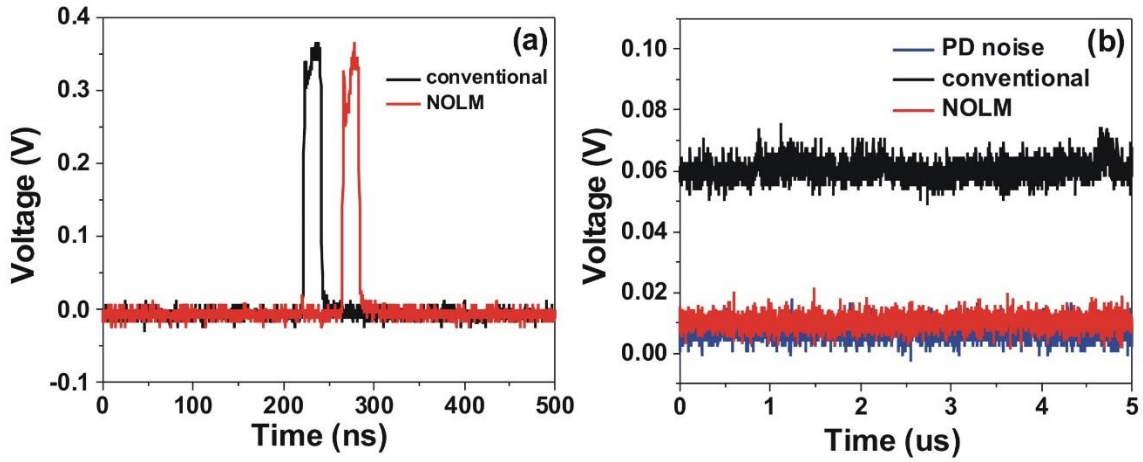

Figure 5.12 (a) 20ns optical pulse generated by using the conventional setup and NOLM; (b) The CW components obtained by using the conventional setup and NOLM.

To verify that the NOLM could improve the ER of optical pulse, the peak power of optical pulse and CW leakage power should be known in conventional and NOLM Φ-OTDR setup. Figures 5.12(a) and 5.12(b) show 20 ns optical pulse and the CW leakage light obtained by the conventional setup and the NOLM. The PD background noise is also shown in figure 5.12(b). The optical pulses shown in figure 5.12(a) are measured by using the 3.5 GHz bandwidth PD and 20dB attenuation is added before the PD to prevent the saturation. To compare the CW leakage light in

both cases, the pulse peak power should be adjusted to the same voltage and then the CW leakage light is measured by a low noise and high gain PD with 125 MHz bandwidth. The 3 GHz filter with an insertion loss 3 dB is also added before both PDs to filter out the ASE noise.

To correctly calculate the ER of the optical pulses, the pulse peak power and CW leakage power are required for both cases. PDs should be calibrated to get the relation between electric voltage and optical power since the optical pulse and CW components are measured by PDs in electric voltages. Figures 5.13(a) and 5.13(b) show calibration curves of 3.5 GHz and 125 MHz PDs with a linear conversion between optical power and electric voltage. The red curves in figure 5.13 are the linear fitting curve. The calculated pulse peak power in both cases are 56.04 mW. The CW leakage powers in the conventional setup and the NOLM are 2.1 μW and 0.17 μW respectively. The CW leakage light is effectively suppressed by utilizing the NOLM and the ER is improved from 44 dB to 55 dB.

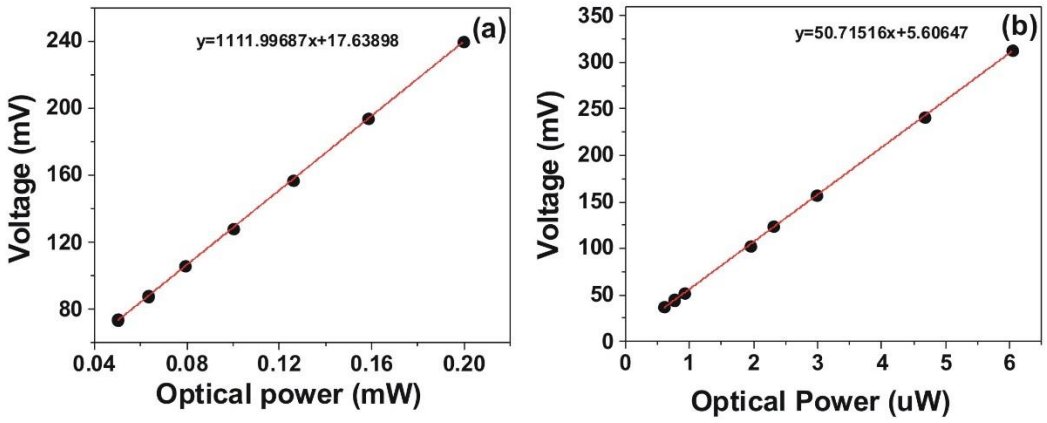

Figure 5.13 The relation between electric voltage and optical power of PD (a):3.5GHz PD; (b) 125MHz PD

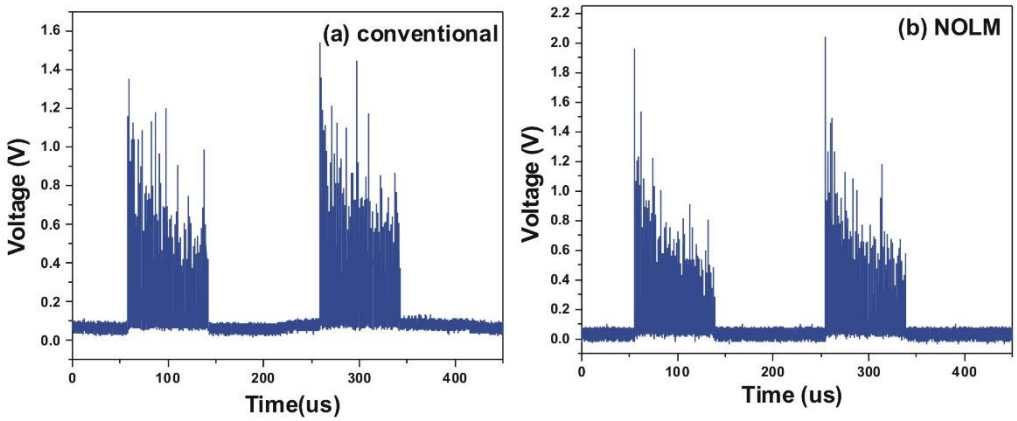

Figure 5.14 The Φ-OTDR traces obtained by (a) conventional setup; (b) NOLM.

The Φ-OTDR optical time domain traces are obtained by using the conventional setup and NOLM, which are shown in figures 5.14(a) and 5.14(b). The two adjacent traces are obtained by using the 20 ns pulse width and 8.4 km single mode fiber. The repetition rate and sampling rate in the experiment is set as 5 kHz and 250 M/s. In the figure 5.14(a), the ripples between two Φ-OTDR traces are caused by the Rayleigh interference induced by CW leakage light which could decrease the SNR of detected signal. For the vibration measurement, the stable and repeatable optical traces are required to identify the vibration location. The instability of Φ-OTDR traces caused by the CW light makes it difficult for vibration sensing. By improving the ER of the optical pulse, the influence of CW light could be almost neglected. After realizing the high ER optical pulse generation, the vibration measurement is performed with NOLM setup. The PZT is inserted in the 7.2 km position and 2 m fiber is wrapped around the PZT. To get the vibration information, 500 trace sequences are collected in the experiment. The vibration location then is obtained by the traces subtraction shown in figure 5.15(a). The zoom in on figure 5.15(a) around the vibration location is shown in figure 5.15(b). The 2 m half width of vibration signal corresponds to the pulse width of 20 ns used in the experiment. Then the power spectrum of vibration signal of 1 kHz is

obtained by performing the FFT at the vibration location shown in figure 5.15(c).

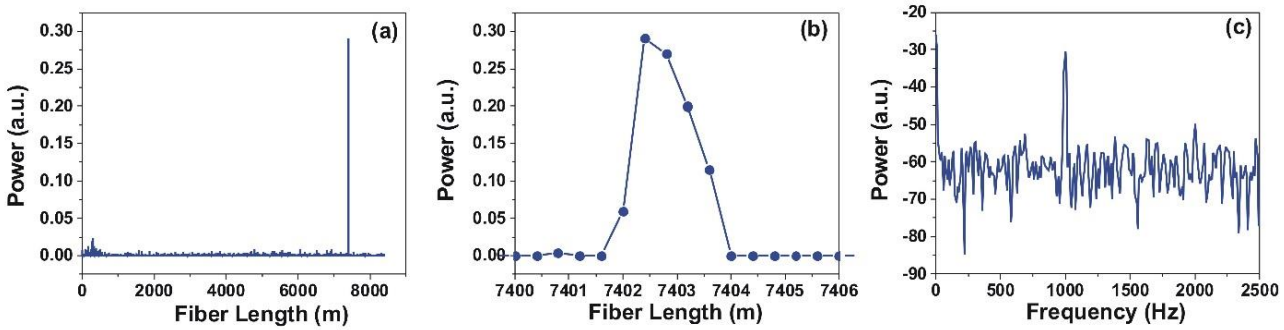

Figure 5.15 (a) Vibration location information; (b) zoom in graph of (a) around the vibration position (c) Power spectrum of vibration 1 kHz

The NOLM based on the Φ-OTDR has been demonstrated for high ER pulse generation. ER is improved from 44 dB to 55 dB by utilizing the NOLM. The 8.4 km and 2 m spatial resolution is also achieved for vibration sensing based on NOLM setup. Compared to the dual EOMs setup, NOLM setup is more cost effective and suitable for practical application. However, the stability of optical pulse generated by NOLM is not as good as the dual EOMs setup because NOLM is very sensitive to the polarization state. In addition, the ER of NOLM is limited by the Rayleigh backscattering in the loop [74]. Thus choosing the proper length of fiber in the loop and gain factor is crucial in the experiment.

5.4 Conclusion

In conclusion, two approaches have been developed for high ER pulse generation. In the dual EOMs configuration, the obtained ER is dependent on the individual ER of the EOM. The generated ER could be very high and the optical pulse is stable but at the expense of setup complexity and higher cost of EOMs. Sensing ranges of 8.4 km and 1.8 km with spatial resolutions of 1 m and 0.5 m are achieved in the dual EOMs setup, respectively. High ER pulse generation

has also been demonstrated with a NOLM which could also effectively suppress the CW light. The ER in this case is improved from 44 dB to 55 dB. By using this setup, vibration sensing along 8.4 km with 2 m spatial resolution is achieved and demonstrated.

Chapter 6

6 Summary and Future work

6.1 Summary

This thesis mainly focuses on developing a distributed optical fiber vibration sensor based on phase-sensitive optical time domain reflectometry (Φ-OTDR). The use of Φ-OTDR for dynamic measurements and the effects involved in its operations, were theoretically and experimentally studied. Three works have been addressed in this thesis for enhancing the performance of a Φ-OTDR sensor system.

Φ-OTDR distributed optical fiber vibration sensor based on the polarization diversity scheme has been proposed. The demonstrated configuration could compensate for position related polarization fading occurring in the conventional coherent detection. A real distributed sensing application for simultaneous multi-events vibration detection can thus be achieved along each position of the sensing fiber with more reliable vibration detection results. The experimental results show that the SNR of two vibration signals are enhanced by 10.9 dB and 8.65 dB compared to the results obtained by a conventional coherent detection scheme.

The piezoelectric sinusoidal vibration signals are theoretically and experimentally evaluated in the Φ-OTDR sensor system. Vibration modulation amplitude measurements then are performed by analyzing the peak value of FFT spectrum at the fundamental frequency and high-order harmonics. The random amplitude fluctuation is suppressed by stabilizing sensor system and the trace to trace correlations varying from 0.83 to 0.94 is obtained in 100 experiment measurements. The standard deviation of amplitude measurements depends on the system noises

and also the PZT vibration induced extra phase and amplitude change.

Two approaches of dual EOMs setup and nonlinear optical fiber loop mirror have been developed to enhance the extinction ratio of optical pulse. The high extinction ratio optical pulse could reduce the intra-band noise and enhance the SNR of Φ-OTDR traces which is desired for the long range and high spatial resolution distributed vibration sensing application. The distributed vibration sensing measurement of 1.8 km fiber length and 0.5 m spatial resolution has been achieved in the dual EOMs setup. Also, the sensing range of 8.4 km and 1m spatial resolution has been demonstrated in the NOLM setup.

6.2 Future work

The following topics are presented for the future improvement of the work developed in this thesis.

The Φ-OTDR based polarization diversity scheme has been demonstrated to eliminate the position dependent polarization fading effect which is more suitable for the multi-events detection. Two vibration signals are simultaneously measured in chapter 3. However, measuring two vibration events is not good enough in the applications. Future work may be done by testing several vibration events at the same time to verify whether the polarization diversity scheme enhances the performance of Φ-OTDR sensor system.

The piezoelectric sinusoidal vibration amplitude measurements have been presented by monitoring the peak value of FFT spectrum. The intensity demodulation makes it easier to recover the signal but it requires the calibration at different positions along the fiber. Coherent balanced detection may be applied in the system to demodulate the phase. Then the amplitude measurement can be obtained by monitoring the phase change at the vibration location.

Bibliography

1. F. USDOT, "FTA.,[2006 Status of the Nation's Highways, Bridges, and Transit: Conditions and Performance]," in *Report to Congress*, 2007),
2. C. Boller, "Structural health monitoring in aeroespace," Advance course on SHM (2009).
3. S. P. Singh, R. Gangwar, and N. Singh, "Nonlinear scattering effects in optical fibers," Progress In Electromagnetics Research **74**, 379-405 (2007).
4. K.-I. Aoyama, K. Nakagawa, and T. Itoh, "Optical time domain reflectometry in a single-mode fiber," Quantum Electronics, IEEE Journal of **17**, 862-868 (1981).
5. A. H. Hartog, "A distributed temperature sensor based on liquid-core optical fibers," Lightwave Technology, Journal of **1**, 498-509 (1983).
6. A. J. Rogers, "Polarization-optical time domain reflectometry: a technique for the measurement of field distributions," Appl. Opt. **20**, 1060-1074 (1981).
7. N. Linze, P. Tihon, O. Verlinden, P. Mégret, and M. Wuilpart, "Development of a multi-point polarization-based vibration sensor," Opt. Express **21**, 5606-5624 (2013).
8. Z. Zhang and X. Bao, "Distributed optical fiber vibration sensor based on spectrum analysis of Polarization-OTDR system," Opt. Express **16**, 10240-10247 (2008).
9. M. E. Froggatt, D. K. Gifford, S. T. Kreger, M. S. Wolfe, and B. J. Soller, "Distributed strain and temperature discrimination in unaltered polarization maintaining fiber," in *Optical Fiber Sensors*, (Optical Society of America, 2006), ThC5.
10. D.-P. Zhou, Z. Qin, W. Li, L. Chen, and X. Bao, "Distributed vibration sensing with time-resolved optical frequency-domain reflectometry," Opt. Express **20**, 13138-13145 (2012).
11. Y. Dong, L. Chen, and X. Bao, "Time-division multiplexing-based BOTDA over 100km sensing length," Opt. Lett. **36**, 277-279 (2011).
12. M. A. Soto, G. Bolognini, F. Di Pasquale, and L. Thévenaz, "Simplex-coded BOTDA fiber sensor with 1 m spatial resolution over a 50 km range," Opt. Lett. **35**, 259-261 (2010).
13. H. Liang, W. Li, N. Linze, L. Chen, and X. Bao, "High-resolution DPP-BOTDA over 50 km LEAF using return-to-zero coded pulses," Opt. Lett. **35**, 1503-1505 (2010).
14. W. Li, X. Bao, Y. Li, and L. Chen, "Differential pulse-width pair BOTDA for high spatial resolution sensing," Opt. Express **16**, 21616-21625 (2008).
15. H. Ohno, H. Naruse, M. Kihara, and A. Shimada, "Industrial applications of the BOTDR optical fiber strain sensor," Optical fiber technology **7**, 45-64 (2001).
16. D. Iida and F. Ito, "Detection sensitivity of Brillouin scattering near Fresnel reflection in BOTDR measurement," J. Lightwave Technol. **26**, 417-424 (2008).
17. T. Kurashima, T. Horiguchi, H. Izumita, S.-i. Furukawa, and Y. Koyamada, "Brillouin optical-fiber time domain reflectometry," IEICE transactions on communications **76**, 382-390 (1993).

18. G. Bolognini, J. Park, M. A. Soto, N. Park, and F. Di Pasquale, "Analysis of distributed temperature sensing based on Raman scattering using OTDR coding and discrete Raman amplification," Measurement Science and Technology **18**, 3211 (2007).

19. J. Dakin, D. Pratt, G. Bibby, and J. Ross, "Distributed optical fibre Raman temperature sensor using a semiconductor light source and detector," Electronics Letters **21**, 569-570 (1985).

20. H. F. Taylor and C. E. Lee, "Apparatus and method for fiber optic intrusion sensing," (Google Patents, 1993).

21. J. C. Juarez and H. F. Taylor, "Field test of a distributed fiber-optic intrusion sensor system for long perimeters," Appl. Opt. **46**, 1968-1971 (2007).

22. L. Yuelan, Z. Tao, C. Liang, and B. Xiaoyi, "Distributed Vibration Sensor Based on Coherent Detection of Phase-OTDR," Lightwave Technology, Journal of **28**, 3243-3249 (2010).

23. Q. Zengguang, C. Liang, and B. Xiaoyi, "Wavelet Denoising Method for Improving Detection Performance of Distributed Vibration Sensor," Photonics Technology Letters, IEEE **24**, 542-544 (2012).

24. Q. Zengguang, Z. Tao, C. Liang, and B. Xiaoyi, "High Sensitivity Distributed Vibration Sensor Based on Polarization-Maintaining Configurations of Phase-OTDR," Photonics Technology Letters, IEEE **23**, 1091-1093 (2011).

25. Y. Lu, T. Zhu, L. Chen, and X. Bao, "Distributed vibration sensor based on coherent detection of phase-OTDR," Lightwave Technology, Journal of **28**, 3243-3249 (2010).

26. M. Nakazawa, "Rayleigh backscattering theory for single-mode optical fibers," JOSA **73**, 1175-1180 (1983).

27. G. P. Agrawal, *Nonlinear fiber optics* (Academic press, 2007).

28. R. Hui and M. O'Sullivan, *Fiber optic measurement techniques* (Academic Press, 2009).

29. G. P. Agrawal, *Fiber-optic communication systems* (John Wiley & Sons, 2012), Vol. 222.

30. W. Seo, "Fiber Optic Intrusion Sensor Investigation," (1994).

31. L. Shi, T. Zhu, Q. He, and S. Huang, "Effect of laser linewidth on phase-OTDR based distributed vibration sensing regime," in *OFS2014 23rd International Conference on Optical Fiber Sensors*, (International Society for Optics and Photonics, 2014), 91576H-91576H-91574.

32. X. Zhong, C. Zhang, L. Li, S. Liang, Q. Li, Q. Lü, X. Ding, and Q. Cao, "Influences of laser source on phase-sensitivity optical time-domain reflectometer-based distributed intrusion sensor," Appl. Opt. **53**, 4645-4650 (2014).

33. F. Zhu, X. Zhang, L. Xia, Z. Guo, and Y. Zhang, "Active compensation method for light source frequency drifting in Φ-OTDR sensing system," (2015).

34. X. Hui, S. Zheng, J. Zhou, C. Xu, H. Chi, X. Jin, and X. Zhang, "Electro-optic modulator feedback control in phase-sensitive optical time-domain reflectometer distributed sensor,"

Appl. Opt. **52**, 8581-8585 (2013).

35. Q. He, T. Zhu, X. Xiao, D. Diao, W. Huang, and X. Bao, "Real distributed vibration sensing with high frequency response based on pulse pair," in *OFS2014 23rd International Conference on Optical Fiber Sensors*, (International Society for Optics and Photonics, 2014), 915761-915761-915764.

36. T. Zhu, Q. He, X. Xiao, and X. Bao, "Modulated pulses based distributed vibration sensing with high frequency response and spatial resolution," Opt. Express **21**, 2953-2963 (2013).

37. Q. He, T. Zhu, J. Zhou, D. Diao, and X. Bao, "Frequency response enhancement by periodical non-uniform sampling in distributed sensing," (2015).

38. H. F. Martins, S. Martin-Lopez, P. Corredera, P. Salgado, O. Frazão, and M. González-Herráez, "Modulation instability-induced fading in phase-sensitive optical time-domain reflectometry," Opt. Lett. **38**, 872-874 (2013).

39. Z. Wang, J. Li, M. Fan, L. Zhang, F. Peng, H. Wu, J. Zeng, Y. Zhou, and Y. Rao, "Phase-sensitive optical time-domain reflectometry with Brillouin amplification," Opt. Lett. **39**, 4313-4316 (2014).

40. H. F. Martins, S. Martin-Lopez, P. Corredera, M. L. Filograno, O. Frazao, and M. Gonzalez-Herráez, "Phase-sensitive optical time domain reflectometer assisted by first-order raman amplification for distributed vibration sensing over> 100 km," J. Lightwave Technol. **32**, 1510-1518 (2014).

41. H. Martins, S. Martin-Lopez, M. Filograno, P. Corredera, O. Frazão, and M. Gonzalez-Herraez, "Comparison of the use of first and second-order Raman amplification to assist a phase-sensitive optical time domain reflectometer in distributed vibration sensing over 125 km," in *OFS2014 23rd International Conference on Optical Fiber Sensors*, (International Society for Optics and Photonics, 2014), 91576K-91576K-91574.

42. B. Soller, D. Gifford, M. Wolfe, and M. Froggatt, "High resolution optical frequency domain reflectometry for characterization of components and assemblies," Opt. Express **13**, 666-674 (2005).

43. J. Song, W. Li, P. Lu, Y. Xu, L. Chen, and X. Bao, "Long-Range High Spatial Resolution Distributed Temperature and Strain Sensing Based on Optical Frequency-Domain Reflectometry," Photonics Journal, IEEE **6**, 1-8 (2014).

44. Z. Ding, X. S. Yao, T. Liu, Y. Du, K. Liu, Q. Han, Z. Meng, and H. Chen, "Long-range vibration sensor based on correlation analysis of optical frequency-domain reflectometry signals," Opt. Express **20**, 28319-28329 (2012).

45. Z. N. Wang, J. J. Zeng, J. Li, M. Q. Fan, H. Wu, F. Peng, L. Zhang, Y. Zhou, and Y. J. Rao, "Ultra-long phase-sensitive OTDR with hybrid distributed amplification," Opt. Lett. **39**, 5866-5869 (2014).

46. X. Bao and L. Chen, "Recent progress in Brillouin scattering based fiber sensors," Sensors **11**, 4152-4187 (2011).

47. M. A. Soto, G. Bolognini, and F. D. Pasquale, "Enhanced simultaneous distributed strain

and temperature fiber sensor employing spontaneous Brillouin scattering and optical pulse coding," Photonics Technology Letters, IEEE **21**, 450-452 (2009).

48. Q. Cui, S. Pamukcu, W. Xiao, and M. Pervizpour, "Truly distributed fiber vibration sensor using pulse base BOTDA with wide dynamic range," Photonics Technology Letters, IEEE **23**, 1887-1889 (2011).

49. J. C. Juarez, E. W. Maier, K. N. Choi, and H. F. Taylor, "Distributed Fiber-Optic Intrusion Sensor System," J. Lightwave Technol. **23**, 2081 (2005).

50. D. W. Stowe, D. R. Moore, and R. G. Priest, "Polarization fading in fiber interferometric sensors," Microwave Theory and Techniques, IEEE Transactions on **30**, 1632-1635 (1982).

51. A. D. Kersey, M. J. Marrone, and A. Dandridge, "Polarization diversity detection for fiber interferometers using active feedback control of output polarization-mode selection," Opt. Lett. **15**, 1315-1317 (1990).

52. J. C. Juarez and H. F. Taylor, "Polarization discrimination in a phase-sensitive optical time-domain reflectometer intrusion-sensor system," Opt. Lett. **30**, 3284-3286 (2005).

53. D. Liu, M. Song, and X. Zhang, "Polarization insensitive coherent detection for Brillouin scattering spectrum in BOTDR," Optics Communications **254**, 168-172 (2005).

54. J. Urricelqui, F. Lopez-Fernandino, M. Sagues, and A. Loayssa, "Polarization diversity scheme for BOTDA sensors based on a double orthogonal pump interaction," (2015).

55. J. W. Goodman, "Some fundamental properties of speckle," J. Opt. Soc. Am. **66**, 1145-1150 (1976).

56. J. Ohtsubo and T. Asakura, "Statistical properties of laser speckle produced in the diffraction field," Appl. Opt. **16**, 1742-1753 (1977).

57. S. O. Rice, "Mathematical Analysis of Random Noise," Bell System Technical Journal **23**, 282-332 (1944).

58. E. W. Stacy, "A Generalization of the Gamma Distribution," The Annals of Mathematical Statistics **33**, 1187-1192 (1962).

59. G. H. Ames and W. R. Donat, "Fading statistics in Rayleigh interferometric fiber sensors," in *OFS2014 23rd International Conference on Optical Fiber Sensors*, (International Society for Optics and Photonics, 2014), 915767-915767-915764.

60. C. He, L. Hang, and B. Wu, "Design of a piezoelectric transducer cylindrical phase modulator for simulating acoustic emission signals," Frontiers of Mechanical Engineering in China **2**, 370-373 (2007).

61. H. Jeong, J. Kim, H.-W. Lee, and B. Kim, "Birefringence modulation in fiber-optic phase modulators," Opt. Lett. **19**, 1421-1423 (1994).

62. N. J. Frigo, A. Dandridge, and A. Tveten, "Technique for elimination of polarisation fading in fibre interferometers," Electronics Letters **20**, 319-320 (1984).

63. M. K. Barnoski, M. D. Rourke, S. Jensen, and R. Melville, "Optical time domain reflectometer," Appl. Opt. **16**, 2375-2379 (1977).

64. F. Peng, H. Wu, X.-H. Jia, Y.-J. Rao, Z.-N. Wang, and Z.-P. Peng, "Ultra-long high-sensitivity Φ-OTDR for high spatial resolution intrusion detection of pipelines," Opt. Express **22**, 13804-13810 (2014).

65. A. Masoudi, M. Belal, and T. P. Newson, "A distributed optical fibre dynamic strain sensor based on phase-OTDR," Measurement Science and Technology **24**, 085204 (2013).

66. P. Healey, "Fading in heterodyne OTDR," Electronics Letters **20**, 30-32 (1984).

67. H. Izumita, S. Furukawa, Y. Koyamada, and I. Sankawa, "Fading noise reduction in coherent OTDR," Photonics Technology Letters, IEEE **4**, 201-203 (1992).

68. H. Izumita, Y. Koyamada, S. Furukawa, and I. Sankawa, "Stochastic amplitude fluctuation in coherent OTDR and a new technique for its reduction by stimulating synchronous optical frequency hopping," Lightwave Technology, Journal of **15**, 267-278 (1997).

69. R. L. Filler, "The acceleration sensitivity of quartz crystal oscillators: a review," IEEE Trans Ultrason Ferroelectr Freq Control **35**, 297-305 (1988).

70. B. Nelson, K. Blow, P. Constantine, N. Doran, J. Lucek, I. Marshall, and K. Smith, "All-optical Gbit/s switching using nonlinear optical loop mirror," Electronics letters **27**, 704-705 (1991).

71. K. J. Blow, N. J. Doran, and B. P. Nelson, "Demonstration of the nonlinear fibre loop mirror as an ultrafast all-optical demultiplexer," Electronics Letters **26**, 962-964 (1990).

72. I. N. Duling, "All-fiber ring soliton laser mode locked with a nonlinear mirror," Opt. Lett. **16**, 539-541 (1991).

73. S. Martin-Lopez, M. Alcon-Camas, F. Rodriguez, P. Corredera, J. D. Ania-Castañon, L. Thévenaz, and M. Gonzalez-Herraez, "Brillouin optical time-domain analysis assisted by second-order Raman amplification," Opt. Express **18**, 18769-18778 (2010).

74. A. G. Striegler and B. Schmauss, "Extinction ratio improvement by an advanced NOLM setup," Photonics Technology Letters, IEEE **18**, 1058-1060 (2006).